Human Activities Caused Hypoxia Expansion in a Large Eutrophic 1 **Estuary: Non-negligible Role of Riverine Suspended Sediments** 2 3 Yue Nan¹, Zheng Chen², Bin Wang³, Bo Liang⁴, Jiatang Hu^{1,5,6*} 4 5 ¹ School of Environmental Science and Engineering, Sun Yat-Sen University, 6 7 Guangzhou, 510275, China ² Earth, Ocean and Atmospheric Sciences Thrust, The Hong Kong University of 8 9 Science and Technology (Guangzhou), Guangzhou, 511455, China ³ Department of Oceanography, Dalhousie University, Halifax, Nova Scotia, Canada 10 ⁴ Eco-Environmental Monitoring and Research Center, Pearl River Valley and South 11 12 China Sea Ecology and Environment Administration, Ministry of Ecology and Environment of the People's Republic of China, Guangzhou, 510611, China 13 ⁵ Guangdong Provincial Key Laboratory of Environmental Pollution Control and 14 Remediation Technology, Guangzhou, 510275, China 15 ⁶ Southern Marine Science and Engineering Guangdong Laboratory (Zhuhai), Zhuhai, 16 17 519000, China

Correspondence: Jiatang Hu (hujtang@mail.sysu.edu.cn)

18

21 Abstract

22

23

24

25

26

27

28

29

30

31

32

33

34

35

36

37

38

39

40

41

42

43

44

45

46

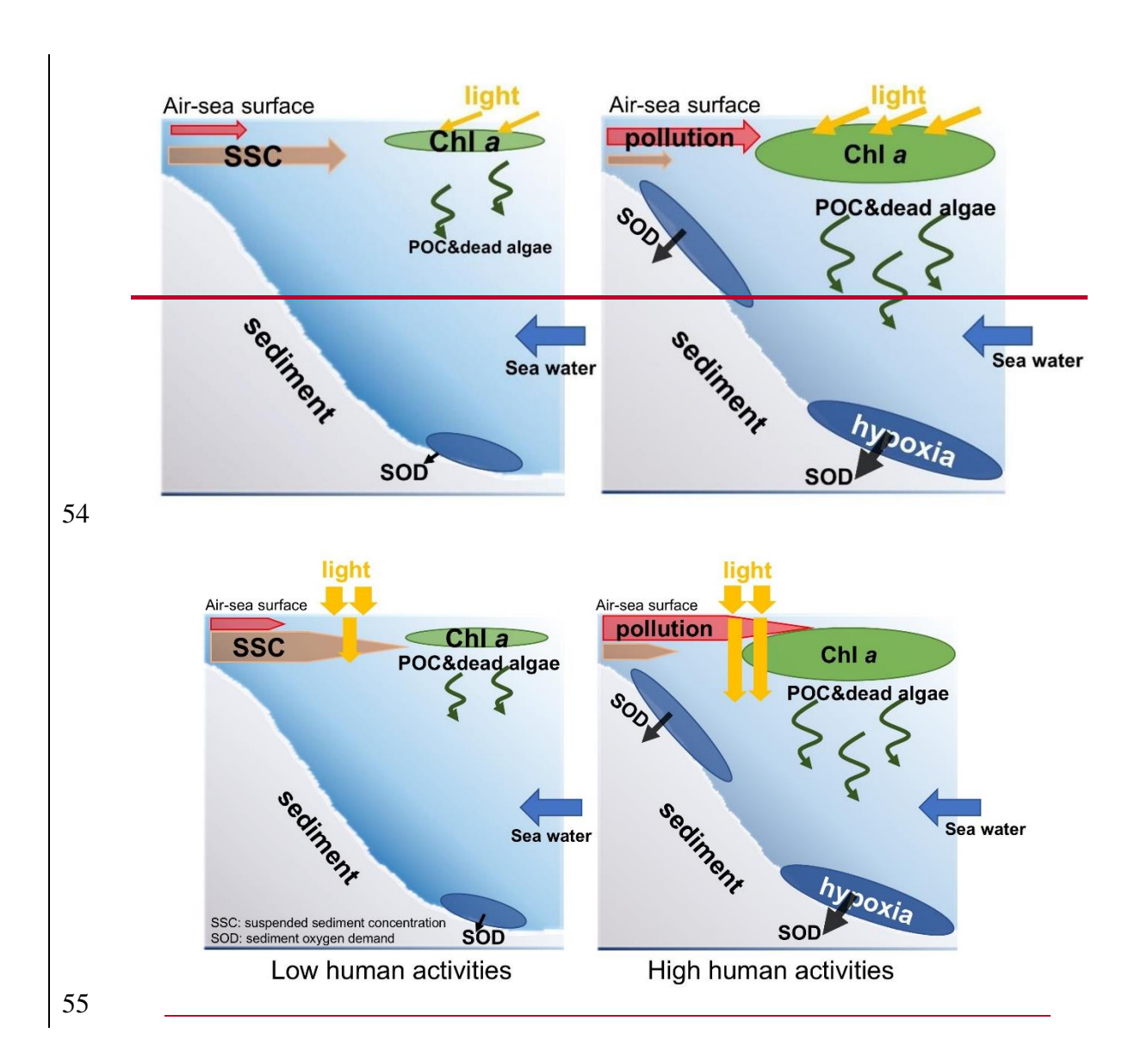
47

48

Increase in riverine nutrient loads was generally recognized as the primary cause of coastal deoxygenation, whereas the role of other riverine factors, especially suspended sediments, has received less attention. This study aims to discern the impacts of anthropogenic alterations in various riverine inputs on the subsurface deoxygenation over the past three decades in a large river-dominated estuary, the Pearl River Estuary (PRE). By utilizing the physical-biogeochemical model, we reproduced the observed dissolved oxygen (DO) conditions off the PRE in the historical period (the 1990s with high-suspended sediments-DO and low-nutrient inputs) and the present period (the 2010s with low-suspended sediments-DO and high-nutrient inputs). Due to the decadal changes in riverine inputs, the PRE has witnessed more extensive and persistent lowoxygen events during summer in the 2020s, with larger spatial extents of ~2926 km² for low oxygen (DO \leq 4 mg/L, increased by \sim 148% relative to the 1990s) and 617 km² for hypoxia (DO \leq 3 mg/L, by 192%) and longer duration (by \sim 15-35 days), evolving into three distinct hypoxic centers controlled by different factors. Model experiments suggested that the decreased riverine DO content (46%) has led to a low-oxygen expansion in the upper regions, accounting for 44% to the total increment. Meanwhile, the increased nutrient levels (100% in nitrogen and 225% in phosphorus) and the declined suspended sediment concentration (60%) have jointly promoted the primary production and bottom oxygen consumptions (dominated by sediment oxygen uptake), thus resulting in a substantial enlargement of low-oxygen area (104%) and hypoxic area (192%) in the lower reaches. Our results revealed a more critical role of the riverine suspended sediment decline in the exacerbation of eutrophication and deoxygenation off the PRE via improving light conditions to support higher local productivity, which could further amplify the effect combined with the growth in nutrients and confound the effectiveness of hypoxia mitigation under nutrient controls. Overall, in the context of global changes in riverine suspended sediments, it is imperative to reassess the contribution of riverine inputs to the coastal deoxygenation worldwide over the past

- 49 decades, given that the impact of suspended sediments has been constantly overlooked
- in relevant investigations.
- 51 **Key words:** Deoxygenation; suspended sediments; nutrient inputs; decadal changes;
- 52 Pearl River Estuary

Graphical Abstract



1. Introduction

56

58

57 Hypoxia emerges when dissolved oxygen (DO) concentration drops below 3 mg/L

in aquatic systems. It is an undesirable phenomenon which can lead to a series of

biological and ecological consequences, such as damaging the habitat for aquatic organisms and imposing detrimental effects on the ecosystem community structure (Diaz and Rosenberg, 2008; Roman et al., 2019). Due to the substantial impacts from human socioeconomic activities, coastal regions have become a hotspot for hypoxia (Breitburg et al., 2018; Pitcher et al., 2021). Moreover, long-term exacerbation of hypoxia with spatial expansion and increased intensity has been frequently reported in estuarine and coastal regions worldwide during the past decades, including the Baltic Sea (Carstensen et al., 2014), the northern Gulf of Mexico (Bianchi et al., 2010), Chesapeake Bay (Murphy et al., 2011), the Yangtze River Estuary (Chen et al., 2017), and the Pearl River Estuary (Hu et al., 2021). Plenty of studies were conducted to reveal the mechanism of hypoxia formation and evolution in coastal regions. It has been widely recognized that coastal deoxygenation is largely attributed to the eutrophication-driven production of organic matters (Su et al., 2017; Wang et al., 2016; Howarth et al., 2011), which sink to the subsurface waters and bottom sediments, leading to intense oxygen depletion (Wang et al., 2014; Hagy et al., 2005). This would induce hypoxia when the density stratification restricts DO replenishment from the surface waters (Wang et al., 2018; Murphy et al., 2011). One important reason underlying eutrophication and hypoxia is the excessive nutrients that are discharged into the water column and stimulate phytoplankton blooms (Cullen, 2015; Wang et al., 2021; Cormier et al., 2023). Human activities, such as dam construction (Bussi et al., 2021) and soil-water conservation measures (Yang et al., 2024) can significantly reduce suspended sediment in estuaries. In addition, an improved light condition, e.g., due to the decreased suspended sediment loads, could also favor the enhancement of local production and hence hypoxia (Ge et al., 2020; Huang et al., 2022). The effects of nutrient and light conditions vary in coastal systems due to different hydrodynamic and topographic features, which makes the formulation of hypoxia mitigation strategies more challenging. Therefore, a quantitative assessment on the importance of these factors in generating hypoxia is crucial for understanding

59

60

61

62

63

64

65

66

67

68

69

70

71

72

73

74

75

76

77

78

79

80

81

82

83

84

85

the primary drivers of hypoxia evolution and for proposing effective countermeasures.

87

88

89

90

91

92

93

94

95

96

97

98

99

100

101

102

103

104

105

106

107

108

109

110

111

112

113

114

A case in point is the Pearl River Estuary (PRE), which is situated in the northern South China Sea and close to the Guangdong-Hong Kong-Macao Great Bay Area (Fig. 1a). Owing to the relatively large nutrient inputs and vertical stratification formed by freshwater plume, hypoxia typically occurs during summer in the bottom waters of the PRE. Before the 2000s, it was an episodic and small-scale issue because of the synergetic effect of shallow topography, high turbidity (Ma et al., 2022), and the intermittent stratification due to periodic disturbance by the tides. However, large-scale occurrences of low oxygen (when DO < 4 mg/L) and hypoxia were frequently reported in recent years. For example, it was estimated that the low-oxygen area within the PRE achieved 1000 km² and 1500 km² during summer in 2010 (Wen et al., 2020) and 2015 (Li et al., 2018), respectively, which were nearly double to that before the 2000s (Li et al., 2020b). Hu et al. (2021) compiled historical observations over four decades to investigate the long-term deoxygenation trend and its spatial expansion in the PRE. They highlighted the significant contributions of increased nutrient and decreased sediment fluxes from the Pearl River to the exacerbation of low-oxygen conditions in the region. Besides, the low-oxygen inflows from the Pearl River could also contribute to the low-oxygen area in the upper estuary (Hu et al., 2021). Nevertheless, a quantitative understanding of their relative contributions to the low-oxygen expansion in the PRE is lacking, particularly in different subregions (Fig.1b) where the mechanisms controlling the low-oxygen conditions are different (Li et al., 2020a). In the upper part of the PRE (Lingdingyang waters), aerobic respiration of terrestrial organic matter plays a greater role (Su et al., 2017; Yu et al., 2020); in the downstream regions of the PRE, deoxygenation is primarily controlled by eutrophication (Yu and Gan, 2022; Chen et al., 2024).

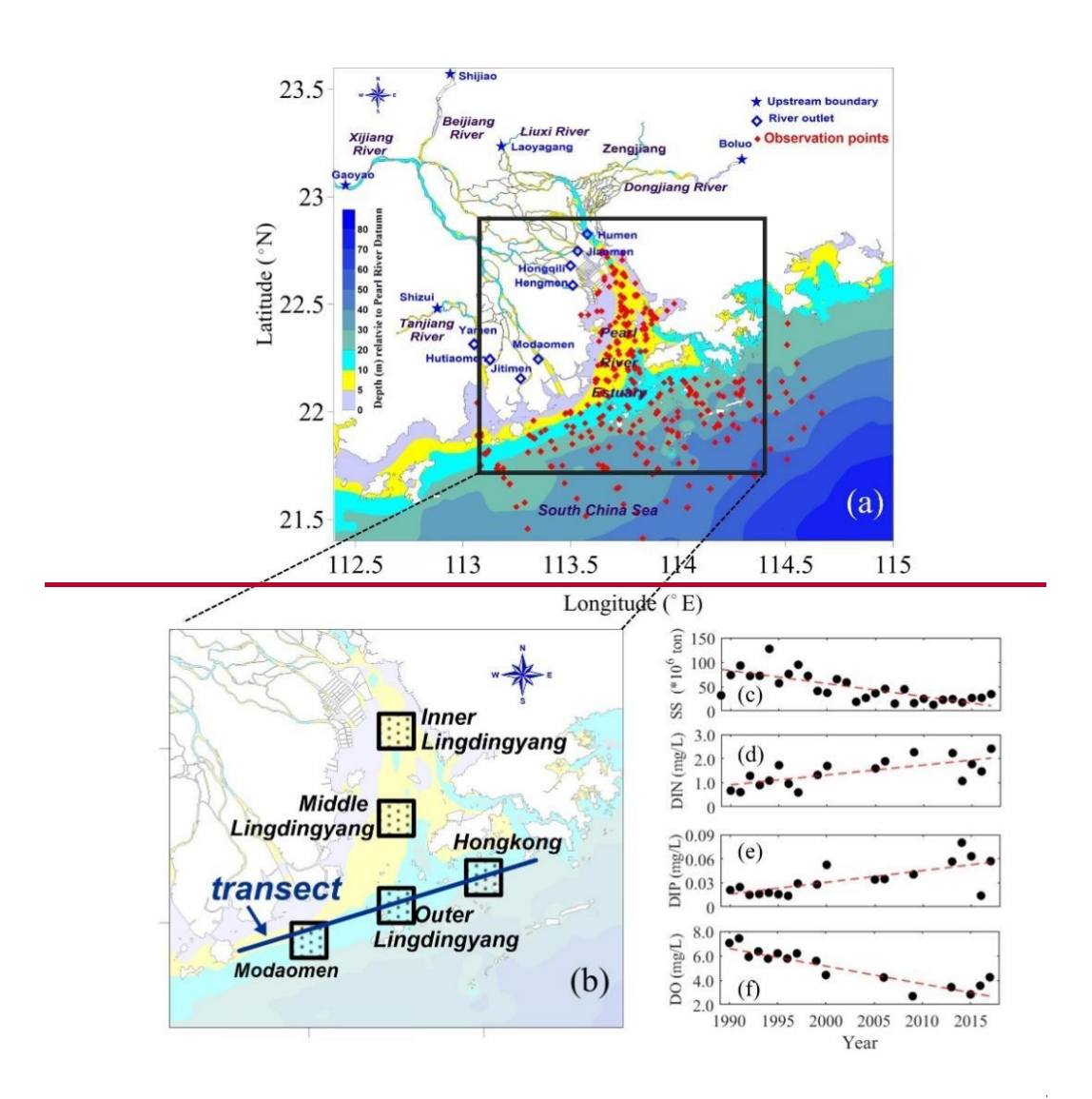
In this study, we used a coupled physical-biogeochemical model to investigate the decadal changes (the 1990s versus the 2010s) in summertime DO contents and related biogeochemical processes in the PRE and to quantify the relative contributions of the

- changing riverine inputs (including nutrients, suspended sediments, and oxygen content;
- Fig. 1c-f) to the long-term expansion of low oxygen (DO < 4 mg/L) and hypoxia (DO
- < 3 mg/L) in the region.

2. Material and methods

2.1 Study area

The PRE and its adjacent shelf waters (Fig. 1a) represent an estuarine system under intensive human activities. One major anthropogenic impact in the PRE is the terrestrial substances fed by the Pearl River, which is the third largest river in China with an average annual runoff of 3.26×10^{118} m³/Year (Luo et al., 2002), through eight river outlets, including Humen, Jiaomen, Hongqili, Hengmen, Modaomen, Jitimen, Hutiaomen, and Yamen (Fig. 1a). The long-term DO and water quality data used here were collected from open sources (e.g. government websites) and published studies (detailed in Data availability and Table S1 of Supplement). (Table S1). Over the past few decades, the terrestrial inputs from the Pearl River hashave experienced remarkable changes in oxygen content, sediment loads, and nutrients including dissolved inorganic nitrogen (DIN) and dissolved inorganic phosphorus (DIP) (Fig. 1c-f). Consequently, the ecological environments of the PRE have changed significantly.



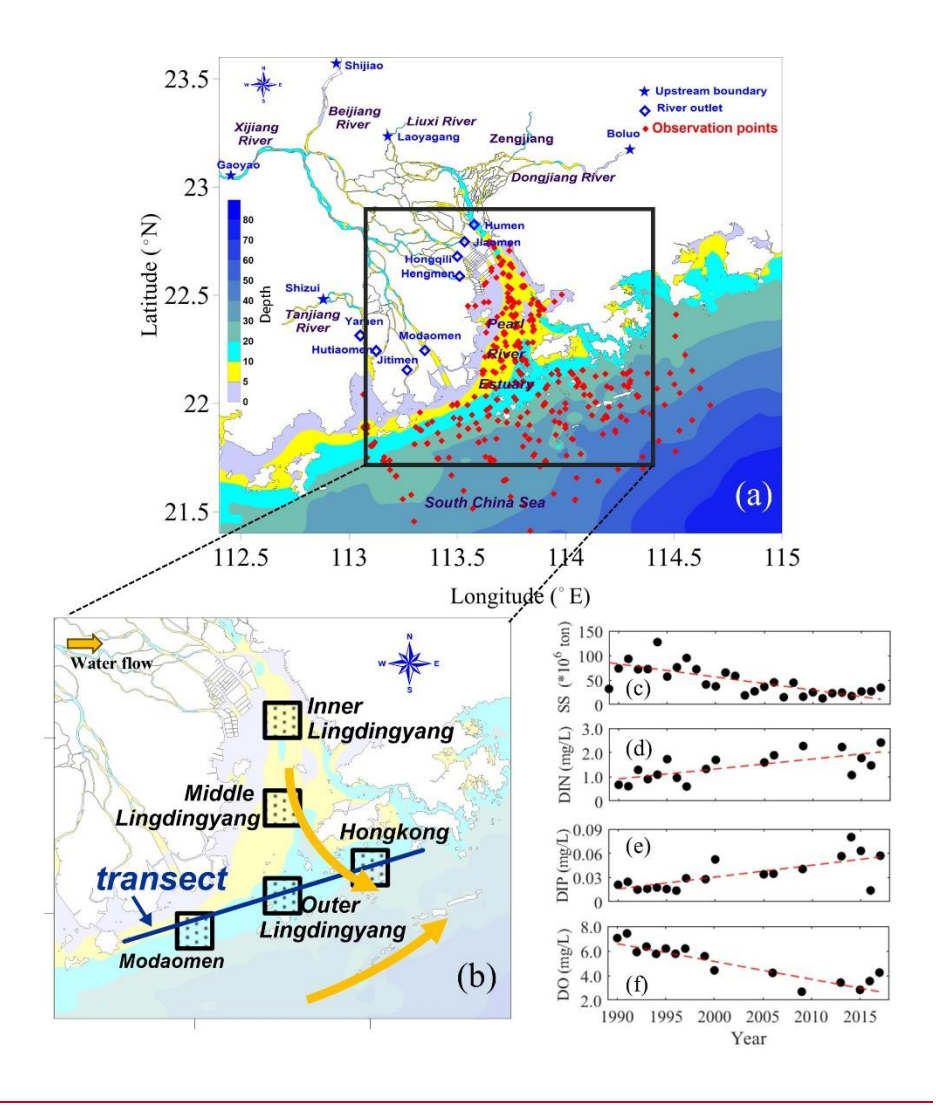


Fig. 1. (a) Study area of the PRE and sampling sites during 1985-2017; (b) five subregions and a transect along the coastal transition zone used for analysis and the water flow direction in the surface water; (c) annual loads of suspended sediments (SS) from the Pearl River; (d-f) the surface-layer (within the upper 2 m of water column) summertime concentrations of nutrients (DIN, DIP) and dissolved oxygen (DO) in the river outlets of the PRE.

In the 1990s, the PRE displayed a low level of eutrophication <u>levels</u>, <u>reflecting</u> <u>limited upstream urbanization at that time. This period also witnessed extensive</u> <u>construction of water infrastructure projects</u>, <u>mostly completed around 2000 (Zhang et al., 2008)</u>, <u>which led to a dramatic reduction in the riverine suspended sediment concentration (SSC)</u>. By the late 1990s, the Pearl River basin contained at least 8636 <u>reservoirs</u>, <u>due to the weak urbanization in the upstream regions and high turbidity</u> <u>because of the absence of large scale hydraulic facilities</u>, e.g., <u>dams</u>, which could block

the suspended sediments from being transported into the estuary. Until the late 1990s, at least 8636 reservoirs were established in the Pearl River basin, the vast majority of which were built after China's reform and opening up in 19801978 (Wu et al., 2016). After the 2000s, with the acceleration of urbanization and construction of hydraulic facilities, the PRE has undergone a significant increase in nutrients and decline in sediment loads (Fig. 1c-e), both of which are favorable for phytoplankton blooms and therefore for eutrophication and hypoxia. These long-term variations of riverine substances have also been reported by Lai et al. (2022) and Hu et al. (2021). In the meantime, the oxygen content in the PRE has exhibited a notable drawdown with significant expansions in low-oxygen extents in recent summers (Fig. 2), which has been revealed by the cruise observations in the PRE (Li et al., 2021; Su et al., 2017; Hu et al., 2021; Lu et al., 2018).

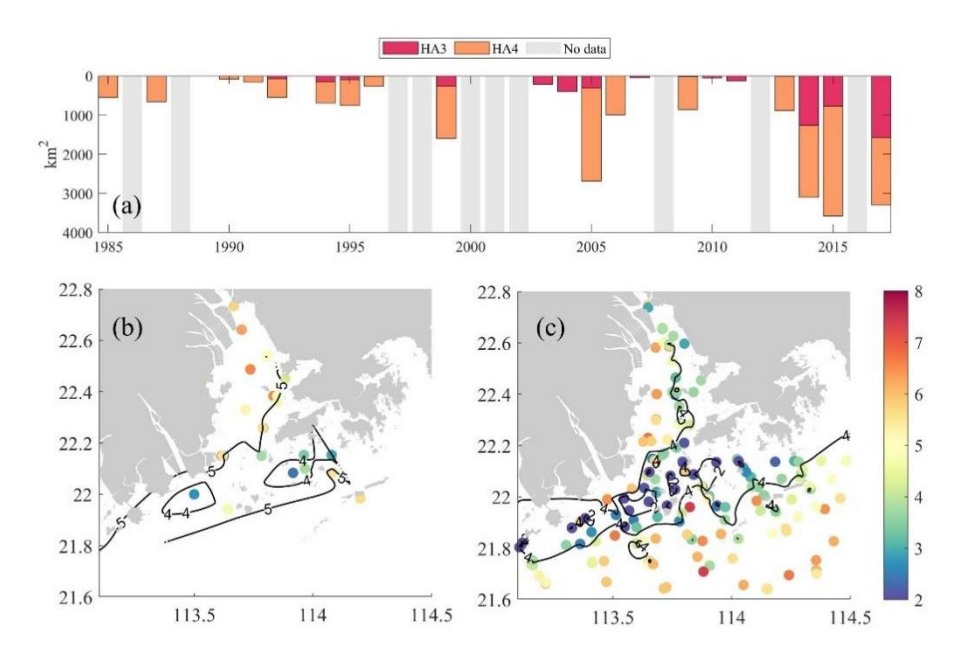


Fig. 2. (a) Interannual variations of low-oxygen area (HA4, DO < 4 mg/L) and hypoxic area (HA3, DO < 3 mg/L) in the bottom waters (\sim 1-2 m above sediments) of the PRE during summer estimated from the cruise observations (note that the grey patches represent the lack of data); spatial distributions of summer-averaged DO concentrations during (b) 1991-1996 and (c) 2013-2017.

2.2 Model settings and validation

166

167

168

169

170

171

172

173

174

175

176

177

178

179

180

181

182

183

184

185

186

187

188

189

190

191

192

2.2.1 Model descriptions and settings

An online 1D-3D coupled physical-biogeochemical model, which has been extensively verified and applied in the PRE (Wang et al., 2017; Wang et al., 2018; Hu et al., 2011; Zhang et al., 2022), was utilized here to reproduce the oxygen dynamics under the long-term changes in riverine nutrients, suspended sediment concentration (SSC), and oxygen content (Fig. 1c-f). This 1D-3D modeling framework integrates a 1D representation of the Pearl River network with a 3D simulation of the Pearl River Estuary and adjacent shelf region, operating in an offline coupling mode. The 1D component numerically solves the Saint-Venant equations using a Preissmann scheme, discretizing the river network into 299 sections with five upstream boundaries (specified as either discharge or water level inputs). The 3D component employs the ECOM model with 16 vertical layers and adaptive horizontal resolution (400m to 3km), forced by tides, atmospheric forcing, and open boundary conditions. The two components exchange fluxes at eight river outlets: the 3D model incorporates river discharge from the 1D model as upstream boundary conditions, while the 1D model uses water levels computed by the 3D model as its downstream boundaries at each time step. This 1D-3D modeling framework was initially developed to investigate nutrient fluxes to the PRE and has been extended and validated to simulate oxygen dynamics and hypoxia in the PRE (Wang et al., 2017; Wang et al., 2018; Hu et al., 2011; Zhang et al., 2022; Chen et al., 2024). For the sake of conciseness in the main text, detailed descriptions on the physical and suspended sediment modules were provided in the Supplement (Text S1). Regarding the biogeochemical module, it is based on the Row-Column Aesop (RCA), which simulates interactive cycles of oxygen, carbon, nitrogen, phosphorus, and silicon in the water column (Fizpartick, 2004). As for the oxygen dynamics, it can be described as follows:

193
$$\frac{\partial DO}{\partial t} = -\mathbf{u} \cdot \nabla DO + \nabla \cdot (\mathbf{D}\nabla DO) + Rea + Phot + WCR + SOD$$
 (1)

$$194 \qquad \frac{\partial DO}{\partial t} = -\left(u\frac{\partial DO}{\partial x} + v\frac{\partial DO}{\partial y} + w\frac{\partial DO}{\partial z}\right) + \frac{\partial}{\partial x}\left(A_{H}\frac{\partial DO}{\partial x}\right) + \frac{\partial}{\partial y}\left(A_{H}\frac{\partial DO}{\partial y}\right) + \frac{\partial}{\partial z}\left(K_{H}\frac{\partial DO}{\partial z}\right) + \frac{\partial}{\partial z}\left(K_{H}\frac{\partial DO}$$

$$195 \quad Rea + Phot + WCR + SOD \tag{1}$$

196 where *DO*-represents the dissolved oxygen concentration (mg/L);
$$-\left(u\frac{\partial DO}{\partial x} + v\frac{\partial DO}{\partial y} + v\frac{\partial DO}{\partial y}\right)$$

197
$$w \frac{\partial DO}{\partial z}$$
 represents the horizontal and vertical advection of oxygen (mg O₂-L⁻¹day⁻¹);

198
$$\frac{\partial}{\partial x} \left(A_H \frac{\partial DO}{\partial x} \right) + \frac{\partial}{\partial y} \left(A_H \frac{\partial DO}{\partial y} \right) + \frac{\partial}{\partial z} \left(K_H \frac{\partial DO}{\partial z} \right)$$
 represents the horizontal and vertical

199 diffusion of oxygen (mg
$$O_2$$
 L^{-1} day where the velocity vector $u =$

respiration, and sediment oxygen demand, respectively (unit: mg
$$O_2$$
 L⁻¹ day⁻¹). The air-

water oxygen exchange is parameterized as:

$$205 \quad Rea = K_a \theta_a^{T-20} \cdot (DO_{sat} - DO)$$
 (2)

where K_a is the surface mass transfer coefficient (m/day), θ_a is the temperature

coefficient, T is the water temperature, and DOsat is dissolve oxygen saturation

208 <u>concentration.</u> The *SOD* is calculated by the sediment flux module (SFM) coupled to

the RCA. The sediment module simulates the sedimentation and remineralization of

organic carbon, nitrogen, and phosphorus, and dynamically estimates the oxygen and

211 nutrient fluxes across the sediment-water interface (Fizpartick, 2004).

The growth of phytoplankton is co-limited by temperature, light, and nutrient

213 conditions. The calculation of gross primary production (GPP, mg C L⁻¹ day⁻¹) of

214 phytoplankton is determined as:

207

209

210

217

215
$$GPP = G_{Pmax} * e^{-\beta(T_{opt}-T)^2} * G_N(N) * G_I(I) * P_c$$
 (32)

where G_{Pmax} is the maximum grow rate of phytoplankton at the optimum temperature

(day⁻¹); T_{opt} is the optimum temperature (°C); β is the shaping coefficients; T is the

218 water temperature (°C); $G_I(I)$ is the light limitation factor; $G_N(N)$ is the nutrient

limitation factor; P_c is the phytoplankton biomass (mg C L⁻¹).

The nutrient limitation factor $(G_N(N))$ -is parameterized as:

$$221 G_N(N) = Min\left(\frac{DIN}{K_{mN} + DIN}, \frac{DIP}{K_{mP} + DIP}, \frac{Si}{K_{mSi} + Si}\right) (\underline{43})$$

- where DIN, DIP, and Si represent the concentration (mg L⁻¹) of dissolved inorganic
- 223 nitrogen (including NO₃⁻ and NH₄⁺), dissolve inorganic phosphorus (PO₄³⁻), and
- dissolve inorganic silicon (SiO₃²⁻), respectively; K_{mN} , K_{mP} , and K_{mSi} represent the
- half-saturation constants (mg L⁻¹) for DIN, DIP, and Si, respectively. It should be noted
- that a higher nutrient limitation factor $G_N(N)$ indicates a weaker nutrient limitation
- 227 effect on phytoplankton growth. Moreover, the nitrogen and phosphorus limitation are
- 228 more significant than silicon limitation within the PRE, thus this study mainly focuses
- on the former.
- 230 The light limitation factor $G_I(I)$ is parameterized as:

231
$$G_I(I) = \frac{e}{k_e H} \left[\exp\left(\frac{-I_0(t)}{I_S} e^{-k_e H}\right) - \exp\left(\frac{-I_0(t)}{I_S}\right) \right]$$
 (54)

232
$$k_e = k_{ebase} + k_c * a_{cchl} * P_c + k_{sed} * SSC + k_{POC} * POC$$
 (65)

233
$$I_0 = I_{surf} * e^{-k_e * H}$$
 (7)(6)

- where H is the depth of water column (m); I_0 is the incident light intensity at the
- segment surface (ly day⁻¹); I_s is the saturating light intensity (ly day⁻¹); k_e is the light
- extinction coefficient (m⁻¹); k_{ebase} is the background light extinction coefficient of
- 237 water (m⁻¹); k_c is the phytoplankton-related extinction coefficient (m² mg⁻¹ Chla); a_{cchl}
- 238 is the ratio of chlorophyll to phytoplankton carbon biomass; k_{sed} is the SSC-related
- extinction coefficient (m² mg⁻¹ SSC); k_{POC} is the POC-related light extinction
- 240 <u>coefficient (m² mg⁻¹ POC)</u>; I_{surf} is the <u>instant instantaneous</u> light radiation received at
- 241 the water surface (ly day⁻¹).
- To estimate the spatial characteristics of light conditions, we also calculated the
- eutrophic depth in the PRE $(H_E, Equation 8)$, which is defined as the water depth
- reached by 1% of the surface light intensity ($\frac{I_{\Box}I_{surf}}{I_{\Box}I_{surf}}$). Basically, a larger eutrophic depth
- indicates a better light condition for phytoplankton growth.

$$I_{surf} * e^{-k_e * H_E} = I_{surf} * 1\%$$
(8)

2.2.2 Model validation

247

248

249

250

251

252

253

254

255

256

257

258

259

260

261

262

263

264

265

266

267

268

269

270

271

272

273

274

The coupled physical-biogeochemical model mentioned above has already been validated against a variety of observations for several periods, which showed good performance in reproducing the physical conditions, suspended sediment dynamics, and biogeochemical cycles in the PRE. We briefly summarized the validation results here. For the physical and suspended sediment modules, Hu and Li (2009) has applied the 1D-3D coupled model to establish 30-day realistic simulations for July 1999 and February 2001. The simulated water levels, discharges, salinity, and SSC agreed well with the observations in the Pearl River network and the PRE for both periods, with correlation coefficients all greater than 0.65 in summer. The simulated SSC at the surface was also compared to satellite remote sensing data, which showed a fairly close spatial pattern and comparable concentration magnitude. Furthermore, Wang et al. (2017) provided an extensive model validation using field data collected from four seasonal cruises in 2006, with high correlations for water levels (> 0.95), salinity (> 0.90) and temperature (> 0.80) and low root-mean-standard-errors between the simulation and observations in summer. Then, the biogeochemical module was established and used to explore the nutrient and oxygen dynamics off the PRE in July 1999 and January-December 2006 (Hu and Li, 2009; Wang et al., 2017). The point-to-point comparisons with the water quality profiles indicated that the biogeochemical module was robust to reproduce the spatial distributions of ammonia, nitrate, phosphorus, oxygen, and chlorophyll a in the PRE. Our model demonstrated strong validation performance by accurately capturing the observed temporal expansion of hypoxia, transitioning from localized bottom hypoxia in the 1990s (Fig. 2b-c) to widespread occurrences in the 2010s (Fig. 5d-e). Initial validation against 1994-1999 summer observations showed close agreement, with simulated low-oxygen (HA4=1179.7 km²) and hypoxic (HA3=211.3 km²) areas matching observational estimates (802±437 km² and 131±84 km²; Fig. 2a, Table 3). For

the 2013-2017 period, the model successfully replicated hypoxia intensification, as evidenced by HA4 expansion to 2925.5 km² aligning with observed 2715±1068 km². Projections to the 2020s indicated HA3 doubling to 617.2 km², remaining within observational uncertainty ranges (901±591 km²; 2013-2017 data), confirming the model's robustness in simulating both historical patterns and emerging hypoxia dynamics. In addition, Wang et al. (2017) has compared the simulated oxygen kinetic terms (including the air-sea re-aeration rate, water-column respiration and production rates, and sediment oxygen demand) with observations in summer, which demonstrated the model's capability in representing the important oxygen source-sink processes (e.g., oxygen consumptions across the sediment-water interface) in the PRE. Detailed model settings and parameters can be found in Wang et al. (2017).

2.3 Model experiments

Based on the well-validated model run in 2006 (Wang et al., 2017), the present study performed diagnostic simulations for two representative periods, characterized by low nutrients and high suspended sediments and oxygen content during 1991-1996 (referring as to the "1990s case"; Table 1) versus high nutrients and low suspended sediments and oxygen content during 2013-2017 (referring as to the "2010s case"). Each case was run from 1 January to 31 August, driven by climatological physical conditions (freshwater discharges and wind speeds detailed in Text S1 of the Supplement) averaged over 1990-2017 and by mean observed values of riverine water quality components in the corresponding period. Specifically in summertime (a period used for formal analysis here), the riverine concentrations were set to 1.0 mg/L (DIN), 0.02 mg/L (DIP), and 6.5 mg/L (DO) in the 1990s case, while they were set to 2.0 mg/L, 0.065 mg/L, and 3.5 mg/L in the 2010s case (Table 1). The riverine SSC was specified at 40 mg/L in the 2010s according to the in-situ observation near the Humen outlet in 2015 summer (Chen et al., 2020), and was set to 100 mg/L in the 1990s based on the ratio of the sediment loads between the 1990s and the 2010s (2.5 times). Long-term

monitoring at river outlets showed no significant temporal trend in COD compared to the marked increases in nutrients and decreases in DO, indicating stable oxygen-consuming OM inputs. We therefore maintained constant OM concentrations between study periods (organic carbon: 2 mg/L; organic nitrogen: 0.2 mg/L; organic phosphorus: 0.03 mg/L), consistent with published historical observations (Wang et al., 2018). Furthermore, three additional model scenario simulations were conducted in order to disentangle the individual impact of each varying riverine input on the summer deoxygenation off the PRE. The setting of each scenario was identical to that of the 1990s case except that the riverine nutrients, SSC, and DO were separately replaced by the representative value in the 2010s (referring as to the "High-nutrient case", "Low-SSC case", and "DO-restore case", respectively; Table 1).

Table 1. Riverine inputs (in unit of mg L-1) for model experiments.

Cases	DIN	DIP	DO	SSC
1990s	1.0	0.020	6.5	100
2010s	2.0	0.065	3.5	40
High-nutrient	2.0	0.065	6.5	100
Low-SSC	1.0	0.020	6.5	40
DO-restore	2.0	0.065	6.5	40

3. Results

3.1 Responses of eutrophication to human-induced changes in

the PRE

3.1.1 Long-term variations in water quality distributions

To examine changes in eutrophication (a key process affecting DO dynamics) and its influential factors during summer in the PRE, we compared the simulated distributions of SSC, nutrients, Chl *a*, and POC in the surface waters between the 1990s

and the 2010s cases (Fig. 3) as well as their vertical integrations in subregions (Table 2). Model results showed that the surface SSC within the PRE largely declined during the two periods. In the 1990s, SSC maintained at a high level in the inner Lingdingyang Bay (see its location in Fig. 1b), ranging from 70.0 to 100.0 mg/L (Fig. 3a). Due to the particle sinking as waters advected downstreamconsecutive sinking along with water transport, SSC dropped has decreased to ~10.0 mg/L in the lower reaches of the PRE in the 1990s. While in the 2010s, the riverine sediment loads have remarkably decreased, resulting in a corresponding drawdown in SSC downstream (Fig. 3b-c). Overall, the vertically-integrated SSC content in the inner Lingdingyang Bay and lower PRE dropped by 56.1% and 45.6%-47.3% to 244.5 mg/m² and 38.4-69.2 mg/m², respectively (Table 2). In terms of nutrients, the variation induced by riverine inputs was also evident during the two periods, acting on the main estuary in association with the spreading of the river plume. As shown, the DIN content in the 1990s was mostly below 1.5 mg/L within the entire PRE (Fig. 3d). With respect to the 2010s, the DIN concentration has increased by 0.8 mg/L and 0.2 mg/L in the surface waters of the upper Lingdingyang Bay and the lower PRE, respectively (Fig. 3e-f). The vertically-integrated DIN mass has increased by 41.9%-102% in the PRE (Table 2). A similar situation occurred with respect to DIP, with its content increasing from 0.04 mg/L in the 1990s to 0.07 mg/L in the 2010s in the high-DIP area adjacent to the middle Lingdingyang Bay (Fig. 3g-i). In terms of vertical integration, DIP increased by 9%-108%, with the lowest increases

located in the Hong Kong waters downstream of the estuary (Table 2).

323

324

325

326

327

328

329

330

331

332

333

334

335

336

337

338

339

340

341

342

343

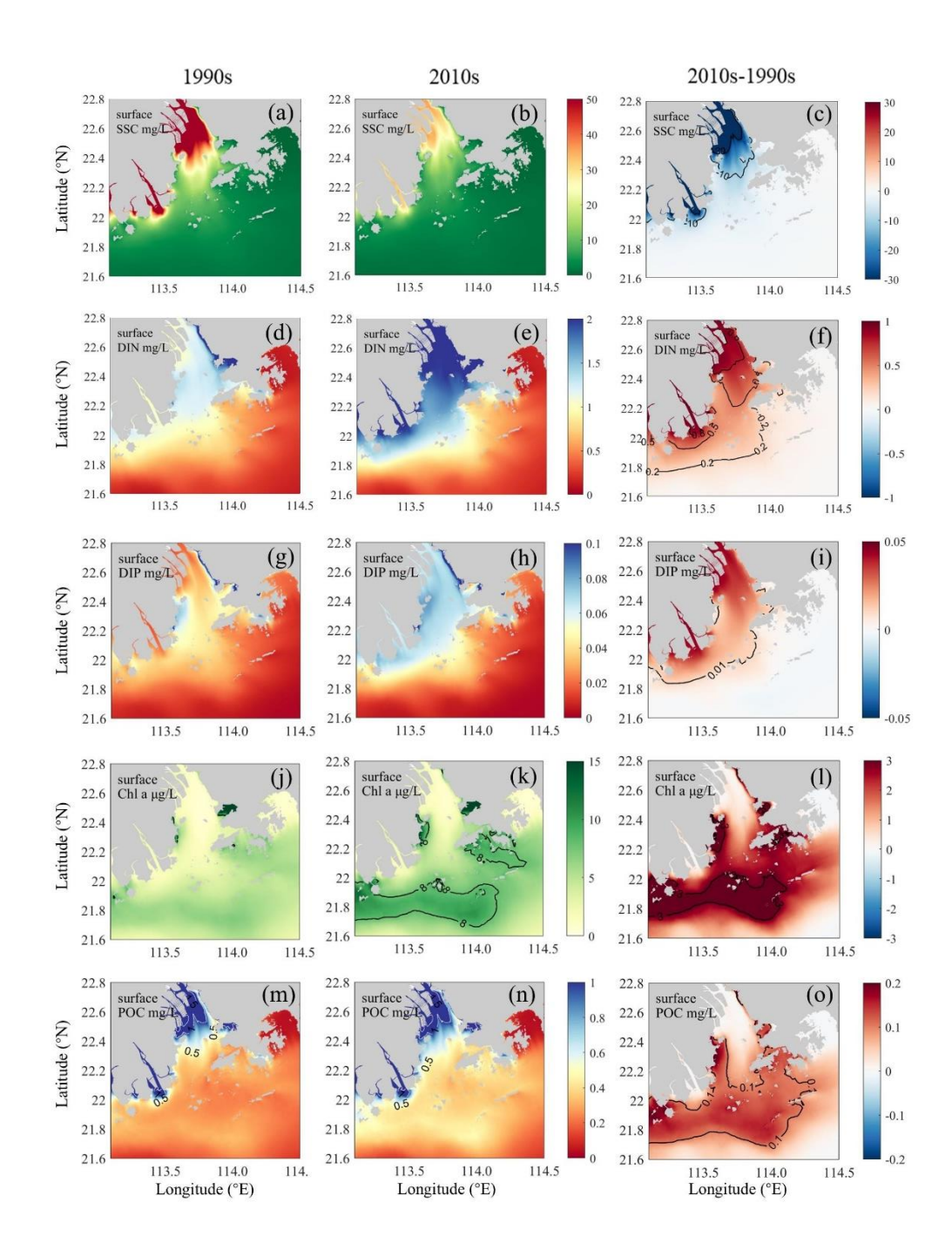


Fig. 3. Simulated distributions of (a-c) SSC, (d-f) DIN, (g-i) DIP, (j-l) Chl a, and (m-o) POC concentrations in the surface waters of the PRE for the 1990s (left panels) and the 2010s (middle panels) as well as their differences (right panels).

Table 2. Vertical integrations of DIN, DIP, SSC, Chl a, and POC contents; nutrient limitation index and euphotic depth; and DO concentrations, low-oxygen frequency (HF4), hypoxia frequency (HF3), and oxygen consumption rates in the bottom waters for subregions of the PRE (see locations in Fig. 1b) during the 1990s and the 2010s.

Cashing	Inner		Middle		Modaomen	en	Outer			04040XX
Subregions	Lingdingyang Bay	ang Bay	Lingding	Lingdingyang Bay	sub-estuary	ıry	Lingding	Lingdingyang Bay	nong no	nong waters
Cases	1990s	2010s	1990s	2010s	1990s	2010s	1990s	2010s	1990s	2010s
$DIN (mg m^{-2})$	6.58	12.24	5.42	9.20	4.89	7.62	5.17	7.92	3.62	5.14
$DIP (mg m^{-2})$	0.23	0.48	0.34	0.48	0.55	0.71	0.56	99.0	0.51	0.56
Nutrient limitation index	0.94	0.97	0.95	0.97	0.92	0.94	0.91	0.93	0.83	0.85
$SSC (mg m^{-2})$	556.5	244.5	332.9	164.6	120.4	63.4	127.7	69.2	9.07	38.4
Euphotic depth (m)	-1.3	-2.3	-2.0	-4.2	-9.5	-11.2	-11.8	-15.2	-20.7	-21.0
$\mathrm{Chl}\ a\ (\mathrm{\mu g\ m^{-2}})$	5.0	7.1	11.7	22.9	39.4	70.4	40.7	72.9	74.3	108.9
$POC \text{ (mg m}^{-2}\text{)}$	8.6	8.64	8.8	5.31	4.82	6:39	5.33	6.85	6.21	7.91
Bottom DO (mg L ⁻¹)	4.55	3.52	4.31	3.90	3.50	2.84	4.96	4.12	4.36	3.52
HF4	25.0%	79.7%	26.8%	65.2%	84.5%	99.1%	4.5%	49.3%	20.5%	61.1%
HF3	6.5%	27.6%	4.8%	10.1%	25.2%	56.5%	3.5%	9.1%	4.8%	21.4%
WCR (mg O_2 L ⁻¹ day ⁻¹)	-0.38	-0.45	-0.20	-0.25	-0.09	-0.11	-0.07	-0.09	-0.06	-0.07
$SOD \ (mg \ O_2 \ L^{-1} \ day^{-1})$	-1.72	-1.62	-0.89	-0.89	-0.24	-0.46	-0.28	-1.12	-0.91	-1.48

Note: HF4 (frequency of DO < 4 mg L⁻¹); HF3 (frequency of DO < 3 mg L⁻¹).

In response to changes in light (affected by the SSC content) and nutrient conditions, phytoplankton biomass has substantially grown in the 2010s, indicated by the increased Chl *a* concentration. In the 1990s, the phytoplankton biomass was at a low level, with the Chl *a* generally below 8.0 μg/L in the surface waters (Fig. 3j). As for the 2010s, significant phytoplankton blooms were found along the Modaomen subestuary, outer Lingdingyang Bay, and Hong Kong waters (Fig. 3k-l), with the vertically-integrated Chl *a* content rising by 31.0 μg/m² (by 78.7% compared to the 1990s), 32.2 μg/m² (79.1%), and 34.6 μg/m² (46.6%), respectively (Table 2). As a result of the elevated primary production, a great amount of organic matter was produced in the PRE. Spatially coupled to the growth of Chl *a* (Fig. 3l), the POC content has significantly increased in the 2010s, especially in the lower PRE (Fig. 3m-o), with the vertically-integrated concentration increasing by 1.5-2.0 mg/m² (by 27.4%-32.6% compared to the 1990s) over the water column (Table 2).

3.1.2 Long-term variations in nutrient and light limitations

The primary production in the PRE was controlled by the synergistic effects of nutrient and light conditions. We calculated the nutrient limitation factor and the eutrophic depth to quantify the intensity of nutrient limitation and light limitation on algae growth. It should be noted that a smaller nutrient limitation index and a shallower eutrophic depth represent a stronger nutrient limitation and a stronger light limitation, respectively. Results showed that the nutrient limitation exhibited a distinct estuary-shelf gradient, in which the Hong Kong waters experienced more severe nutrient limitation than the Modaomen sub-estuary and Lingdingyang Bay (Fig. 4a, c). Specifically, the nutrient limitation index decreased from the upper estuary (0.94) to the Hong Kong waters (0.83) in the 1990s. By contrast, the light limitation has attenuated along the river plume transport, largely ascribed to the decreased SSC (Fig. 3a-b). Compared to the Hong Kong waters, the regions adjacent to river outlets underwent more severe light limitation, shown by the eutrophic depth (Fig. 4b) increasing from the Lingdingyang Bay (1.3 m) and Modaomen sub-estuary (9.5 m) to the Hong Kong

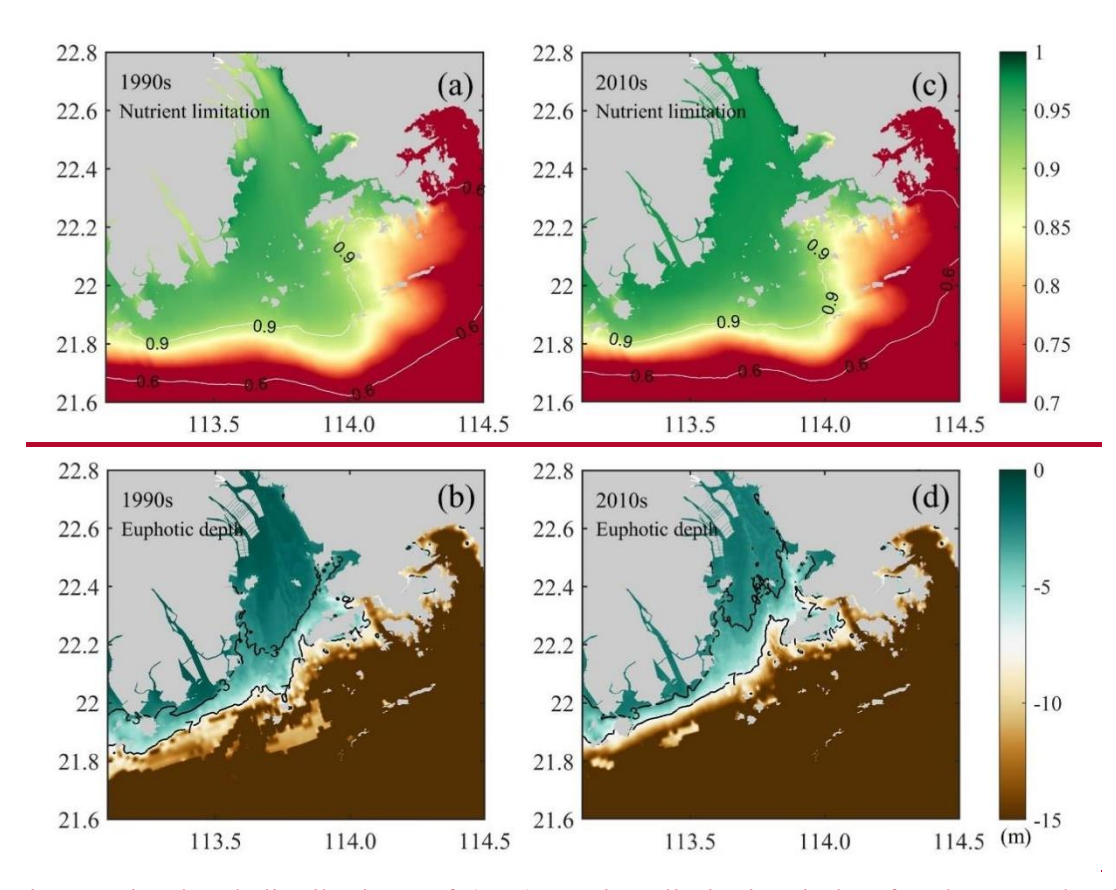


Fig. 4. Simulated distributions of (a, c) nutrient limitation index for the growth of phytoplankton and (b, d) euphotic depth (in unit of m) in the 1990s and the 2010s.

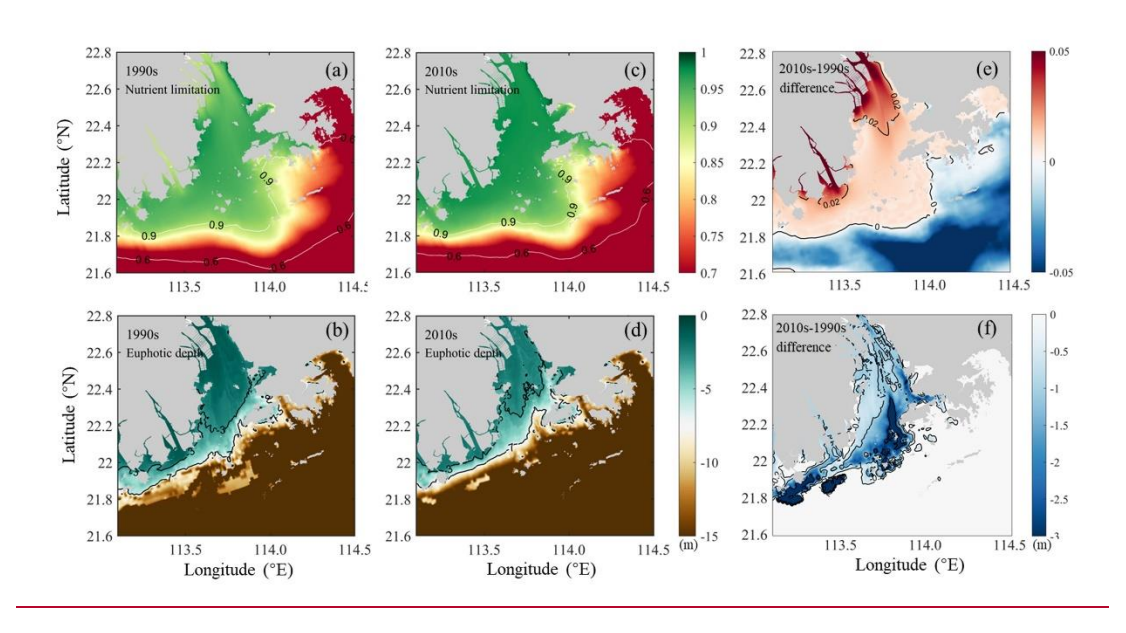


Fig. 4. Simulated distributions (a, c) and difference (e) of nutrient limitation index for the growth of phytoplankton in the 1990s and the 2010s; (b, d) euphotic depth and its difference (e) (in unit of m) in the 1990s and the 2010s.

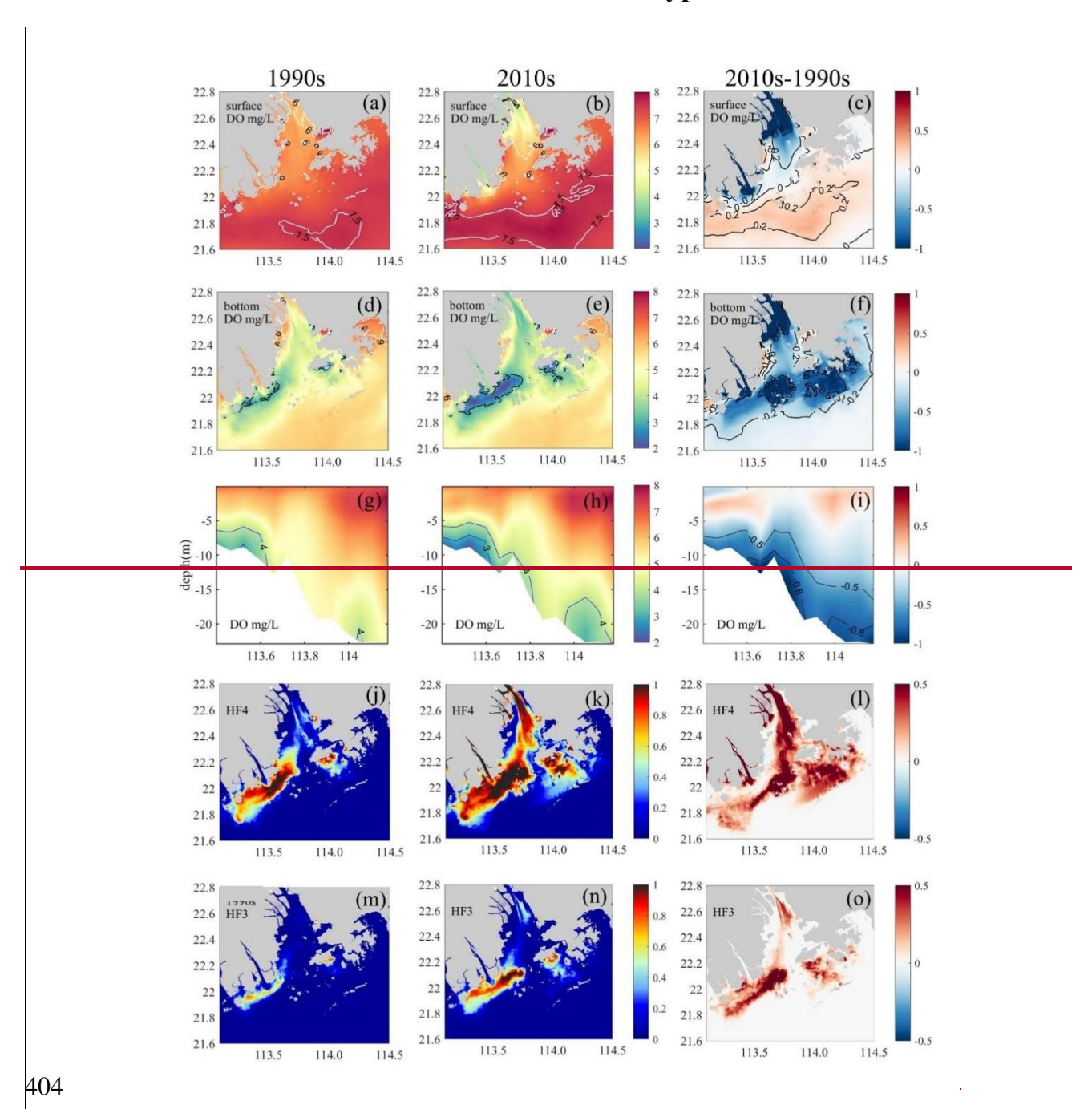
Due to the growth in nutrient loads, nutrient limitation haswas_relieved in the 2010s. For instance, the nutrient limitation index in the Hong Kong waters has increased to 0.85 (by 2.4% of the 1990s) in the 2010s (Table 2). In comparison, the relief of light limitation was more evident with the reduced riverine suspended sediments. The deepening of the euphotic depth in the Lingdingyang Bay was significantly greater than that in the lower estuary (Fig. 4b, d). In the inner Lingdingyang and middle Lingdingyang Bays, the euphotic depth increased by 1 m and 2.2 m (by 76.9% and 110.0% relative to the 1990s, Table2), respectively. The alterations in light conditions in the remaining area were relatively minor, with the eutrophic depth increasing to 11.2 m (by 17.9%) in the Modaomen sub-estuary and to 21 m (by 1.4%) in the Hong Kong waters during the 2010s (Table 2).

3.2 Responses of DO dynamics to human-induced changes in

402 the PRE

403

3.2.1 Variations in DO distributions and hypoxia occurrences



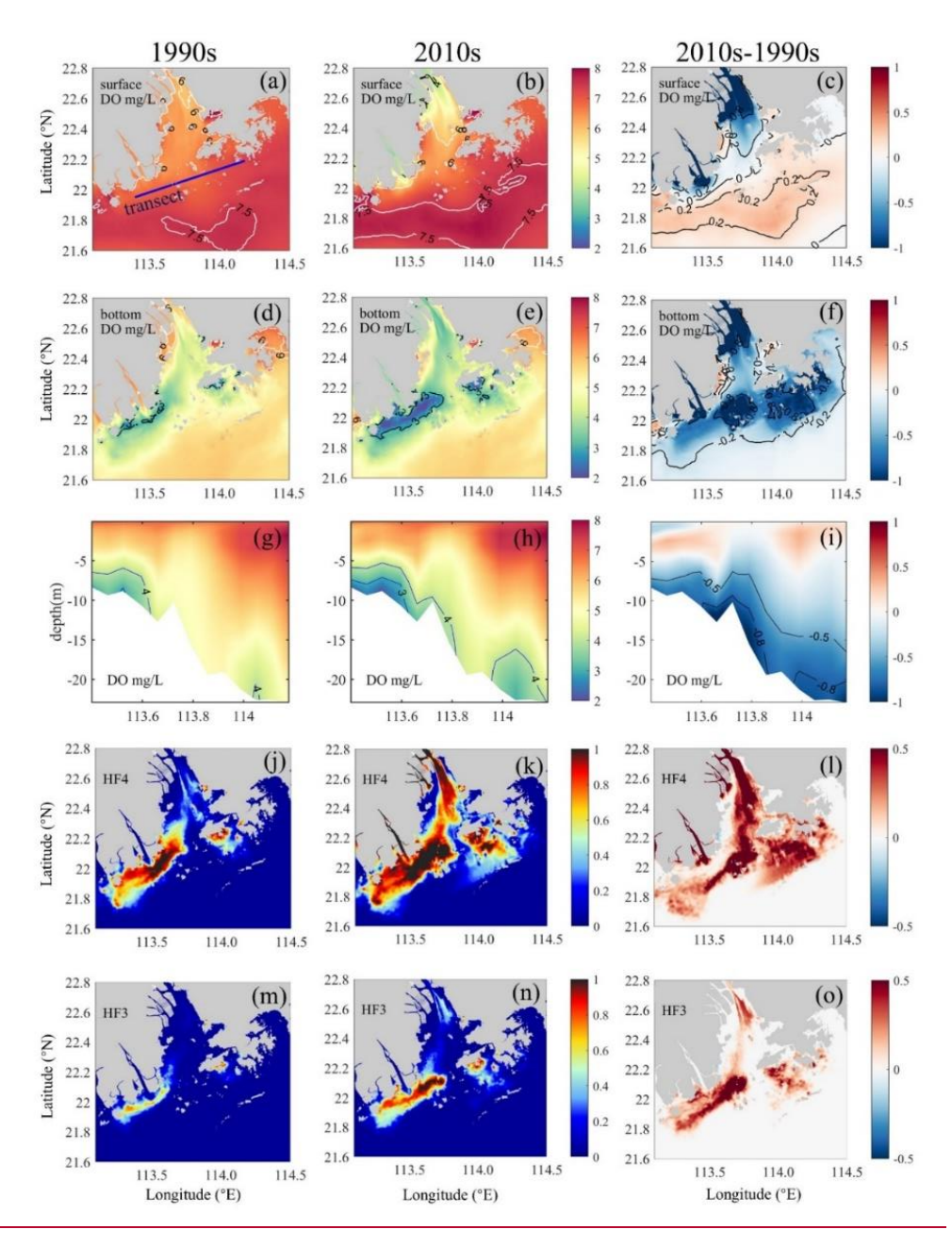


Fig. 5. (a-c) Surface DO and (d-f) bottom DO distributions, (g-i) vertical DO distributions along the transect (see its location in panel a)(see its location in Fig. 1b), and (j-l) low-oxygen frequency (HF4, DO < 4 mg/L) and (m-o) hypoxia frequency (HF3, DO < 3 mg/L) in the bottom waters of the PRE for the 1990s (left panels) and the 2010s (middle panels) as well as their differences (right panels). Note that hypoxia frequency is calculated as the number of hypoxic days divided by the total number of days in the study period, yielding a dimensionless ratio (range: 0–1).

|

Our model revealed distinct temporal shifts in summertime DO patterns and hypoxia distribution (Fig. 5). The surface DO in the 1990s was generally higher than 6

416 mg/L, increasing trend towards the shelf regions (Fig. 5a). By the 2010s, surface DO 417 levels had increased by 0.2-0.3 mg/L (Fig. 5b-c), with an oxygen-enriched zone in the lower PRE correlating with high Chl a (Fig. 3k), though new low-oxygen zones (DO 418 419 <4 mg/L) emerged near river outlets due to reduced Pearl River DO influx.</p> 420 Bottom water simulations captured the hypoxia expansion from small-scale 1990s 421 events (Fig. 2b-c) to widespread 2010s occurrences (Fig. 5d-e). Initial hypoxia 422 clustered along the western PRE (Modaomen sub-estuary; Fig. 5d), with simulated 423 HA4 (1179.7 km²) and HA3 (211.3 km²) (Table 3) matching observations (802±437 424 km² and 131±84 km²; 1994-1999 summers; Fig. 2a). By the 2010s, hypoxia intensified throughout Lingdingyang Bay and Hong Kong waters, with bottom DO declining to 425 426 2.8-4.1 mg/L (Table 2). Simulated HA4 expanded 1.5-fold to 2925.5 km² (Table 3), 427 consistent with observed 2715±1068 km² (2013-2017; Fig. 2a). HA3 doubled to 617.2 428 km² by the 2020s, comparable to observed 901 ± 591 km² (2013-2017). 429 Our model results demonstrated significant changes in the spatial pattern of 430 summertime DO and hypoxia incidences from the past to the present (Fig. 5). The surface DO concentration in the 1990s was generally higher than 6 mg/L and exhibited 431 432 an increasing trend towards the shelf regions (Fig. 5a). While in the 2010s, the surface 433 DO has undergone an evident increase by 0.2-0.3 mg/L (Fig. 5b-c), with an oxygen-434 enriched zone in the lower PRE, which was closely coupled to the surface high Chl a 435 value (Fig. 3k). However, low-oxygen events (DO < 4 mg/L) have appeared in the surface waters adjacent to the river outlets in the 2010s (Fig. 5b) due to the low DO 436 437 influx from the Pearl River along with the freshwater discharge. 438 In the bottom waters, the observed shift from small-scale hypoxia in the 1990s to extensive hypoxia in the 2010s (Fig. 2b-c) was well reproduced by our model (Fig. 5d-439 440 e). In the 1990s, the low-oxygen events were primarily concentrated along the western 441 side of the PRE (i.e. the Modaomen sub-estuary and adjacent waters; Fig. 5d). The 442 simulated low-oxygen area (HA4) and hypoxic area (HA3) were approximately 1179.7 km² and 211.3 km² (Table 3), respectively, which is consistent with the observational 443

estimates of 802 ± 437 (mean ± standard deviation) and 131 ± 84 km² during the summers of 1994-1999 (Fig. 2a). The low-oxygen conditions have considerably worsened over the estuary in the 2010s (Fig. 5e-f), especially evident in the inner Lingdingyang Bay, outer Lingdingyang Bay, and Hong Kong waters. The bottom DO levels have dropped to 2.8 4.1 mg/L on average in the five subregions (Table 2). Simultaneously, the simulated low-oxygen area (HA4) has increased to ~1.5 times larger than that in the 1990s, reaching 2925.5 km² (Table 3). The enlarged low-oxygen coverage in our model is consistent with the observational estimates of 2715 ± 1068 km²-during 2013-2017 (Fig. 2a). Besides, the simulated hypoxic area (HA3) has approximately increased by twofold and reached 617.2 km² in the 2020s, which is also comparable to the observational estimates of 901 ± 591 km²-during 2013-2017.

Table 3. Simulated low-oxygen (HA4, DO < 4 mg/L) and hypoxic (HA3, DO < 3 mg/L) areas in the bottom waters of the PRE and their changes relative to the 1990s.

Cases	HA4 (km ²)	Percentage of change	HA3 (km ²)	Percentage of change
1990s	1179.7	/	211.3	/
2010s	2925.5	+148%	617.2	+192%
High-nutrient	1542.6	+31%	282.5	+34%
Low-SSC	1737.0	+47%	412.4	+95%
DO-restore	2409.7	+104%	617.2	+192%

Note: The calculation in percentage of change is: $(HA_x-HA_{1990s}) / HA_{1990s}$, where x represents each case.

In addition, our model accurately replicated the two observed hypoxic centers along the coastal transition zone (Modaomen sub-estuary and Hong Kong waters; Fig. 2b-c), revealing distinct spatiotemporal deoxygenation patterns (Fig. 5g-o). During the 1990s, both centers exhibited limited low-oxygen zones, with Hong Kong waters showing <1 m thick DO <4 mg/L layers (Fig. 5g). Low-oxygen (HF4) and hypoxic (HF3) conditions persisted 18-76 days (20.5%-84.5% frequency) and 4-23 days (4.8%-25.2%) respectively during summer months (Fig. 5j,m; Table 2).

By the 2010s, hypoxic thickness increased substantially to ~1.5 m at Modaomen and ~5 m (~4 m thicker than 1990s) at Hong Kong waters (Fig. 5h). Event durations prolonged to 55-89 days (61.0%-99.1% HF4) and 19-51 days (21.4%-56.5% HF3) respectively (Fig. 5k, n; Table 2), demonstrating intensified and prolonged hypoxia.

In addition, the two observed hypoxic centers along the coastal transition zone (i.e., the Modaomen sub-estuary and Hong Kong waters; Fig. 2b-c) were also successfully reproduced by our model, showing heterogeneous deoxygenation features in terms of spatial extents and duration (Fig. 5g-o). In the 1990s, the low-oxygen conditions in these two centers were confined to a relatively small extent, especially in the Hong Kong waters, where the simulated thickness of low oxygen (DO < 4 mg/L) was less than 1 m (Fig. 5g). The low-oxygen and hypoxic waters probably sustained for 18-76

days and 4-23 days within the hypoxic centers during the three summer months (June-August), respectively, synonymous with 20.5%-84.5% of low-oxygen occurrences (HF4) and 4.8%-25.2% of hypoxia occurrences (HF3) in summer (Fig. 5j, m; Table 2). As for the 2010s, the estimated thickness of hypoxia in the Modaomen sub-estuary has substantially increased to ~1.5 m, while the low-oxygen thickness in the Hong Kong waters has reached ~5 m (approximately 4 m thicker relative to the 1990s; Fig. 5h). Furthermore, the duration of the low-oxygen and hypoxic events in the 2010s was prolonged, roughly at 55-89 days (61.0%-99.1% of HF4) and 19-51 days (21.4%-56.5% of HF3) in the hypoxic centers (Fig. 5k, n; Table 2), respectively.

3.2.2 Variations in bottom oxygen consumption

To further explore the mechanism of long-term deoxygenation off the PRE, we investigated the oxygen consumption rates and their changes during the two periods (the 1990s versus the 2020s). We specifically focused on the oxygen consumption at the bottom layers covering the 20% of the water depth above the sediments, where the majority of hypoxic events in the PRE occurred (Fig. 5).

As shown in Table 2, the predominant oxygen sink in the bottom waters of the PRE was sediment oxygen demand (SOD) induced largely by the remineralization of organic matter in sediments, whereas water column respiration (WCR) only accounted for 15.2% of the bottom oxygen consumption on average. Over the past three decades, both the WCR and SOD have generally enhanced increased in the PRE, primarily attributed to the growth in local production of organic matter associated with aggravated eutrophication (Fig. 3j-o). Particularly, the SOD in the outer Lingdingyang Bay and Hong Kong waters has remarkably increased from 0.28-0.92 mg O₂ L⁻¹ day⁻¹ in the 1990s to 1.12-1.48 mg O₂ L⁻¹ day⁻¹ in the 2010s (Table 2), which contributed to 80%~95% of the increment in total oxygen consumption. Although the absolute increase of SOD in the Modaomen sub-estuary was comparatively small, the SOD in the 2010s has almost doubled compared to the 1990s, leading to a substantial increase in the occurrence of hypoxic events in this region (Fig. 5d-o).

3.2.3 Disentangling contributions of riverine oxygen, suspended sediments, and nutrient changes on deoxygenation

510

511

512

513

514

515

516

517

518

519

520

521

522

523

524

525

526

527

528

529

530

531

532

533

As detailed in Section 2.3, three scenario simulations were performed to quantify the relative contributions of riverine changes to the decadal low-oxygen expansion in the PRE (Table 1). In general, the riverine impacts on DO and related biogeochemical factors varied significantly between subregions (Figs. 6-7). Specifically, increasing the riverine nutrient levels from the 1990s to the 2020s alone (High-nutrient case) led to a marked drawdown in the bottom DO around the lower PRE (by over 0.2 mg/L relative to the 1990s; Fig. 6a). The DO decline, extending from the Modaomen sub-estuary to the Hong Kong waters, was ascribed to the elevated phytoplankton biomass (Fig. 7b) facilitated by better nutrient conditions, which subsequently sustained stronger bottom oxygen depletions compared to the 1990s (Fig. 7c). Among the subregions, the Hong Kong waters was more susceptible to the changes in riverine nutrients as it was subject to comparatively severe nutrient limitation (Table 2). Therefore, with the improvement of nutrient utilization, this region experienced more pronounced deoxygenation in association with significant alterations in Chl a content and SOD (increased by 14.2 μg/m² and 0.26 mg O₂ L⁻¹ day⁻¹, respectively, equivalent to 47.1% and 46.4% of their total increments over the past three decades; Fig. 7). While in the inner Lingdingyang Bay, the increased nutrient inputs only caused a slight change in Chl a content because the phytoplankton growth in this region was mostly light limited due to high water turbidity (Table 2). The concomitant changes in SOD and bottom DO were fairly small as well. Collectively, the high-nutrient scenario alone resulted in a 31% and 34% growth in the area affected by low oxygen (HA4) and hypoxia (HA3) relative to the 1990s, respectively (Table 3).

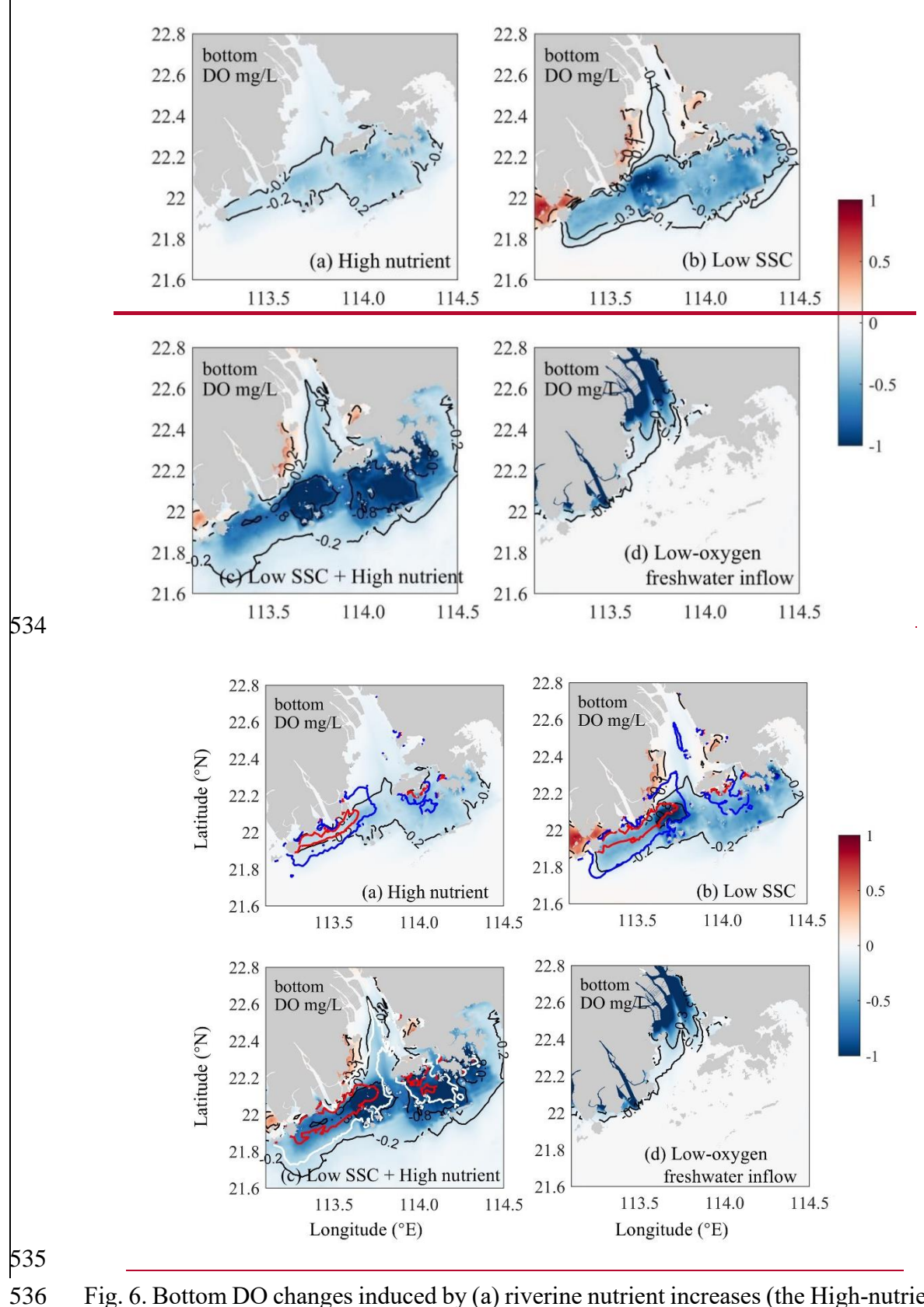
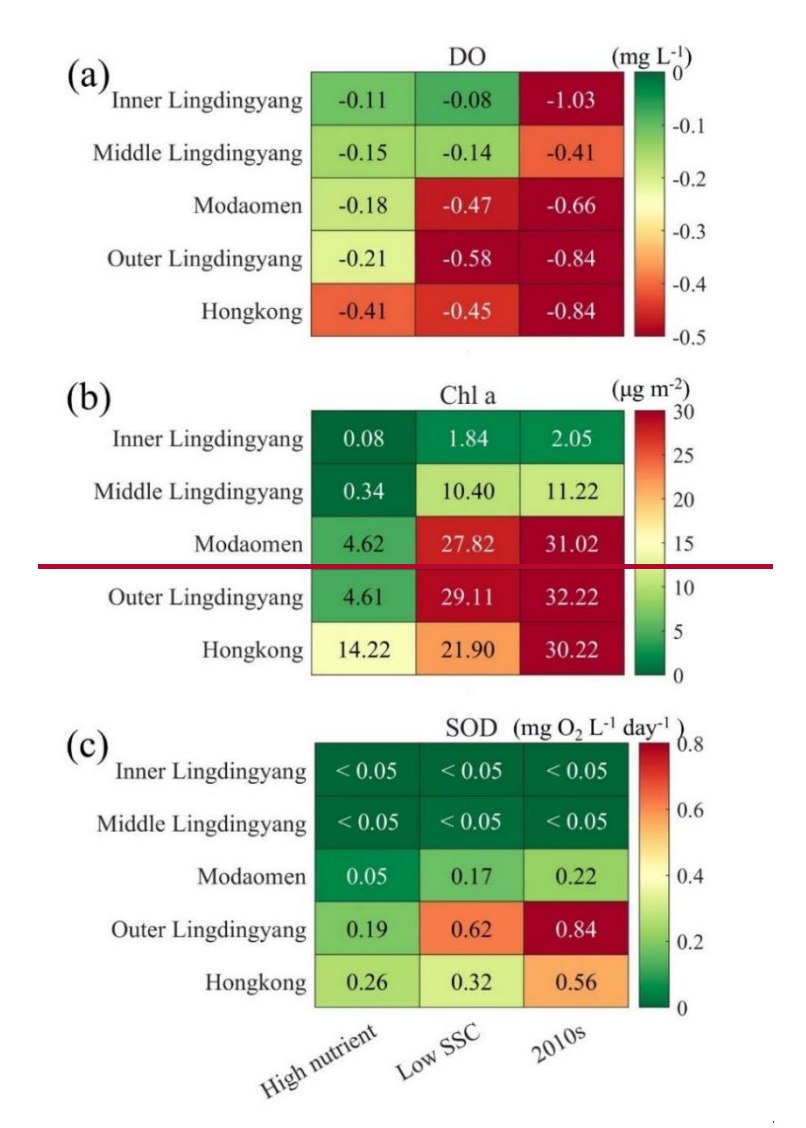


Fig. 6. Bottom DO changes induced by (a) riverine nutrient increases (the High-nutrient case minus the 1990s case), (b) riverine SSC declines (the Low-SSC case minus the 1990s case), (c) the combined effects of nutrient increases and SSC declines (the DO-restore case minus the 1990s case), and (d) riverine DO declines (the DO-restore case



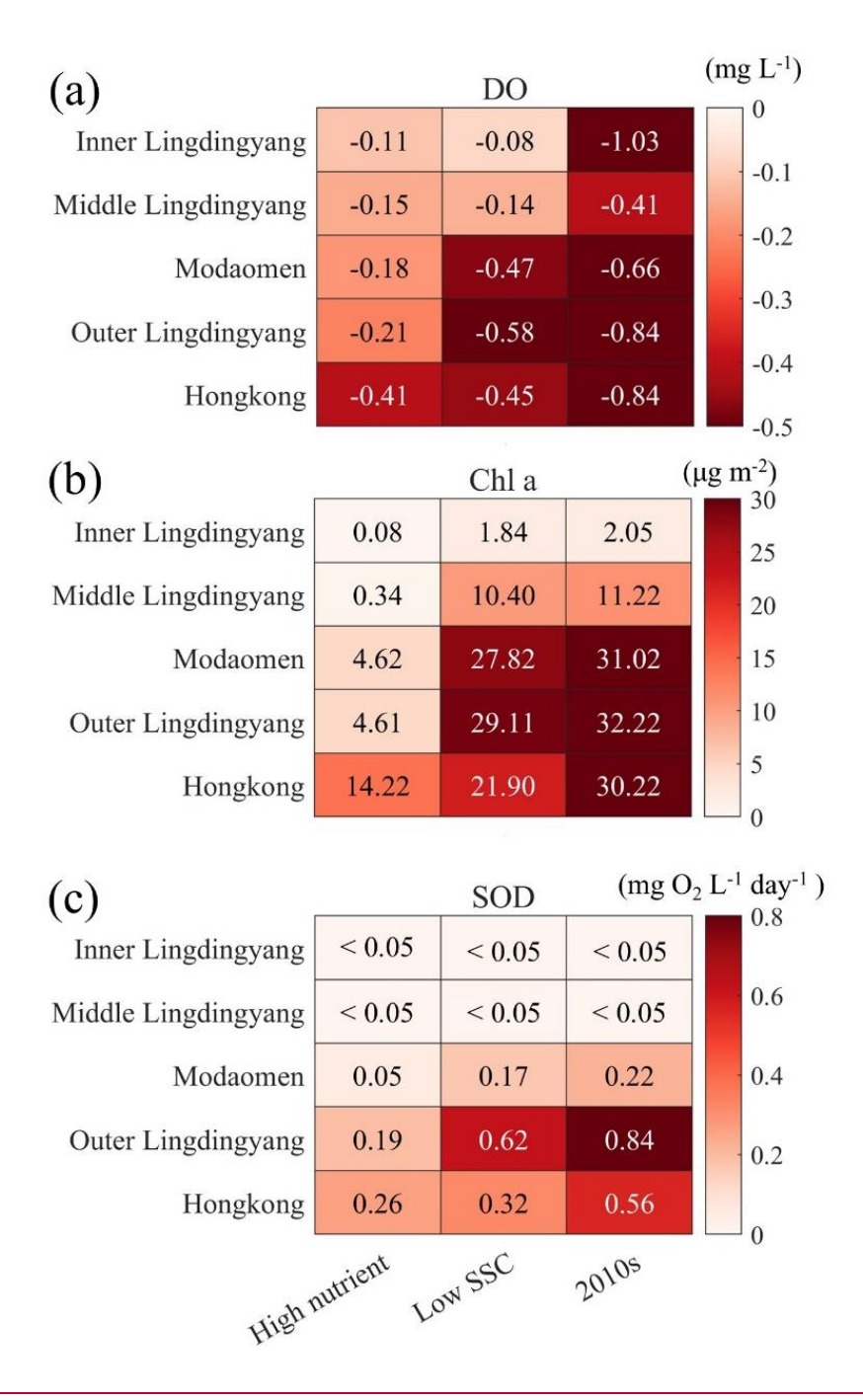


Fig. 7. Changes of (a) bottom DO concentration, (b) vertically-integrated Chl a content, and (c) SOD in subregions of the PRE for the High-nutrient, the Low-SSC, and the 2010s cases relative to the 1990s case.

Compared with the High-nutrient case, reducing the riverine suspended sediment loads from the 1990s to the 2020s alone (Low-SSC case) imposed a greater impact on the DO conditions, causing more extensive and intense deoxygenation through the PRE (Fig. 6b). Apparent DO decline (exceeding 0.3 mg/L relative to the 1990s) occurred

within the lower PRE, similar to that of the changing riverine nutrients described above. This is also attributed to the intensified SOD (with an increment of 0.17-0.62 mg O₂ L⁻ ¹ day⁻¹, accounting for 57.1%-77.3% of the total increment during the two periods; Fig. 7c), accompanied by a prominent increase in Chl a content (by $21.9-29.1 \, \mu \text{g/m}^2$, accounting for 72.4%-90.3% of the total increment; Fig. 7b) due to the improved light condition (the relief of light limitation; Table 2). The SSC-induced changes in these biogeochemical factors were more pronounced in the outer Lingdingyang Bay and Modaomen sub-estuary than in other regions including the Hong Kong waters, which coincided with the alterations in deoxygenation among the subregions (Fig. 7). Overall, under the low-SSC scenario the low-oxygen area (HA4) and hypoxic area (HA3) expanded by 47% and 95% compared to the 1990s, respectively (Table 3). As shown in Figure 7 and Table 3, the combined effect of reducing SSC and increasing nutrient inputs (DO-restore case) led to a significant expansion of low-oxygen conditions, with hypoxic areas (HA4) and low-oxygen areas (HA3) reaching 2409.7 km² and 617.2 km², respectively. This combined effect exceeded the sum of changes induced by individual river inputs, highlighting the non-linear interaction between SSC and nutrient loading. In regions such as Outer Lingdingyang and Hong Kong, the combined effect was amplified, while in regions such as Inner and Middle Lingdingyang, the combined effect was less than the sum of individual effects. The growth of phytoplankton is not a linear process in response to various influencing factors; instead, these factors interact cumulatively. Therefore, when different factors are combined, their combined effect can exceed the impact of individual factors acting alone. In addition, it is important to note that the low-SSC-induced exacerbation could be further escalated by superimposing with the effect of high nutrient inputs (Fig. 6c). As shown, the combined actions of decreasing SSC and increasing nutrients (DO-restore case) promoted a larger area of bottom waters off the lower PRE to develop into a low oxygen or hypoxic state, yielding a substantial expansion of low-oxygen conditions (reaching 2409.7 km² of HA4 and 617.2 km² of HA3; Table 3) that eventually exceeded the sum of changes

552

553

554

555

556

557

558

559

560

561

562

563

564

565

566

567

568

569

570

571

572

573

574

575

576

577

578

induced by individual riverine input.

With respect to the influence of altered riverine DO influx, it could be deduced from the difference between the 2010s and the DO-restore cases (Fig. 6d). There was a considerable DO decrease (by over 0.8 mg/L) in the bottom waters adjacent to the river outlets (also in the surface waters) owing to the low-oxygen inflows from the upstream river channels. The impact of these low-oxygen waters was largely restricted within the upper Lingdingyang Bay under the effects of air-sea reoxygenation and water-column mixing along with the river plume transport. Collectively, reducing the riverine DO content from the 1990s to the 2020s alone resulted in an enlargement of low-oxygen area by nearly 515.8 km² (derived by subtracting the HA4 of the 2010s case from that of the DO-restore case; Table 3).

4. Discussion

4.1 Impacts of decadal changes in riverine inputs on deoxygenation off the PRE

By integrating long-term observations with physical-biogeochemical model simulations, we revealed significant bottom-water deoxygenation in the Pearl River Estuary over the past three decades, driven by changes in riverine inputs. From the 1990s to 2020s, summer inflows of DIN and DIP increased by ~100% and ~225%, while SSC decreased by ~60% due to human activities like dam construction (Liu et al., 2022) and reforestation (Cao et al., 2023). Concurrently, oxygen depletion from terrestrial pollutants reduced riverine DO concentrations by 46% (Ma et al., 2024). These shifts collectively intensified bottom-water low-oxygen conditions in PRE (Fig. 5), with model simulations showing a 148% expansion in summer low-oxygen areas (DO < 4 mg/L) and a 192% decrease in hypoxic areas (DO < 3 mg/L). Low-oxygen events also become more persistent, lasting longer (~15-35 days during June-August) and expanding vertically by ~1-4 m and (Table 3). By combining the long term

observations with simulations from the physical-biogeochemical coupled model, we have elucidated the subsurface deoxygenation and associated mechanisms driven by changes in a variety of riverine inputs over the past three decades in a typical eutrophic estuarine system, namely the Pearl River Estuary (PRE). With the rapid socio-economic development, the inorganic nitrogen and phosphorus contents flowing into the PRE during summer have approximately increased by 100% and 225% from the historical period (1990s) to the present period (2020s), respectively (Table 1). Also, the riverine SSC has decreased by ~60%, consequent to the intense human activities such as dam construction (Liu et al., 2022) and reforestation (Cao et al., 2023). Besides, the amplified oxygen depletion fueled by terrestrial pollutants discharged into the upstream rivers has led to a lower riverine DO concentration (dropped by 46%) entering the estuary (Ma et al., 2024). These alterations have jointly triggered more extensive and persistent low-oxygen conditions in the bottom waters of the PRE (Fig. 5). Based on our model estimation, the summertime low-oxygen (DO < 4 mg/L) and hypoxic (DO < 3 mg/L) areas in the PRE have risen by 148% and 192% during the two periods, respectively (Table 3), together with a significant increase in the vertical thickness (expanding upwards by ~1-4 m) and the duration (extending by ~15-35 days during June-August) of low-oxygen events.

606

607

608

609

610

611

612

613

614

615

616

617

618

619

620

621

622

623

624

625

626

627

628

629

630

631

632

633

More interestingly, the PRE has developed three distinct hypoxic centers (including the inner Lingdingyang Bay, Modaomen sub-estuary, and Hong Kong waters) controlled by different dominant factors, which renders the deoxygenation problem in this region as a great reference for estuaries and coastal systems worldwide. Specifically, the impact of riverine low-oxygen waters was confined within the upper estuary close to the river outlets, leading to a ~44% increase in the low-oxygen area relative to the 1990s. Such local low-oxygen issue could be mitigated to a large extent if the riverine DO recovered to a comparatively higher level (e.g., ~6.5 mg/L in the 1990s) according to the DO-restore scenario (Fig. 6d). Reduced water turbidity downstream facilitates the upstream transport of nutrients, promoting eutrophication and oxygen depletion in

the lower reaches, which is highly sensitive to changes in riverine nutrient and sediment inputs. By comparison, the deoxygenation in the lower estuary primarily followed the classic eutrophication-driven paradigm. As indicated in the High-nutrient and the Low-SSC cases, the increased nutrient inputs and declined suspended sediment loads have separately alleviated the nutrient and light limitations on algae growth in the region, thereby stimulating phytoplankton blooms and local production of organic matter to support subsurface oxygen consumption (dominated by sediment oxygen uptake, SOD; Fig. 7).

While previous studies have primarily examined the impacts of riverine inputs of freshwater, nutrients and organic matter, this study provides a comprehensive investigation of how suspended sediment reduction influences estuarine dissolved oxygen dynamics. In the PRE, Our results also indicated that the riverine SSC reduction played a more important role in driving the long-term low-oxygen expansion—in the PRE. Its synergistic effect with the riverine nutrient changes could further amplify the exacerbation of eutrophication and subsequent deoxygenation, resulting in an enlarged growth in the low-oxygen area (by 104%) and hypoxic area (by 192%) that was notably larger than the total of their partial contributions (Table 3), and reached 70% of the total impact from combined SSC, nutrient, and low-oxygen changes (148% low-oxygen expansion).

It is worth mentioning that the relative importance of the riverine nutrient and SSC changes were different between the two hypoxic centers in the lower PRE, depending upon their distances and water flow conditions from the river outlets. Closer to the river outlets, the Modaomen sub-estuary and its surrounding waters (located on the western side of the coastal transition zone off the PRE) possessed a fairly high SSC level, which imposed a stronger light limitation on the growth of phytoplankton in the region, ultimately making the oxygen dynamics more susceptible to the decline in riverine SSC.

Suspended sediments were confined to the coastal area of Modaomen by water currents (Fig. 1b), resulting in a significant decrease in sediment deposition in this region, which

greatly improved light availability, ultimately making the oxygen dynamics more susceptible to the decline in riverine SSC. On the contrary, the Hong Kong waters and adjacent coastal areas (located on the eastern side of the coastal transition zone) far from the river outlets were less affected by the riverine inputs, where the relatively low nutrient levels promoted more sensitive responses of biogeochemical processes (e.g. primary production and SOD) and hypoxia occurrences to nutrient variations. Besides, the complex island topography near Hong Kong (Fig1b) creates hydrodynamic barriers that restrict the offshore transport of suspended sediments.

662

663

664

665

666

667

668

669

670

671

672

673

674

675

676

677

678

679

680

681

682

683

684

685

686

687

688

4.2 Nutrient control and hypoxia mitigation in the context of sediment declines

Our results underscored the substantial spatial variability in the regulation of riverine inputs on deoxygenation, highlighting the need for which implies the necessity for establishing more refined and targeted strategies for hypoxia mitigation. Compared with the riverine nutrients, the regulatory effects influences of SSC on eutrophication and hypoxia have received less attention. It follows that there might be overestimations of the nutrient impacts in the previous studies without considering SSC to ensure the model simulation aligning with the observed deoxygenation. Such an overfitting problem could further lead to an optimistic assessment on the hypoxic mitigation effect under a certain nutrient control plan. Therefore, it is imperative to disentangle or reevaluate the contribution of riverine nutrients and SSC to the coastal deoxygenation over the past decades. As exemplified in our study for the PRE, a more stringent nutrient reduction might be required to curb the deoxygenation issue given the low SSC status at present. This oversight suggests that previous studies may have overestimated nutrient impacts when failing to account for SSC-mediated processes required to align simulations with observed deoxygenation patterns. Such model overcompensation could lead to potentially optimistic assessments of hypoxia mitigation effectiveness under proposed nutrient control plans. It is therefore critical to

disentangle and quantitatively re-evaluate the relative contributions of riverine nutrients versus SSC changes to coastal deoxygenation dynamics over recent decades. As demonstrated in the PRE case study, the current low-SSC regime suggests more stringent nutrient reductions than previously estimated might be required to effectively curb deoxygenation.

689

690

691

692

693

694

695

696

697

698

699

700

701

702

703

704

705

706

707

708

709

710

711

712

713

714

715

716

Furthermore, it should be noted that although the dam constructions in the Pearl River Basin have mostly completed since the 2000s, it is still unclear whether the declining trend of riverine SSC will persist in the future. For instance, the reforestation in recent years has shown to be effective in reducing the summer freshwater discharges and sediment loads in the Pearl River Basin (Cao et al., 2023). Therefore, the role of riverine This evolving context underscores that SSC variations remains critical will continue to play a defining role in future oxygen dynamics, introducing compounding uncertainties for oxygen dynamics in the future, which poses greater challenges and uncertainties for eutrophication and hypoxia mitigation strategies. Similar problems also exist in other estuaries and coastal systems suffering hypoxia. Notably, analogous sediment-oxygen coupling mechanisms are emerging in other hypoxic systems. For example, it was reported that the decrease of riverine SSC (by ~56%) appeared to be the predominated predominant factor for the intensifying eutrophication (with a 61% increase in the Chl a concentration) in the Yangtze River Estuary over the past decades (Wang et al., 2019). In addition, several modelling studies have showed that the dam constructions in the upper regions of Guadiana Estuary have significantly reduced the water turbidity and exacerbated eutrophication in the lower estuary (Domingues et al., 2012; Barbosa et al., 2010). A global-scale survey revealed that the sediment loads in 414 major rivers has approximately decreased by 51% since the 2000s due to human activities (Dethier et al., 2022), suggesting that the deteriorating eutrophication and deoxygenation in the context of sediment declines has become a global concern and merits more attention and investigations in the future.

While our study emphasizes the impacts of reduced suspended sediments, human

activities may conversely increase sediment loads in estuaries. For example, land-use changes such as deforestation (Kasai et al., 2005) or industrialization (Syvitski and Kettner, 2011) may exacerbate soil erosion and sediment transport, leading to higher suspended sediment concentrations in the water. In such cases, light attenuation due to increased turbidity may suppress phytoplankton growth and reduce primary production, thereby mitigating hypoxia.

717

718

719

720

721

722

723

724

725

726

727

728

729

730

731

732

733

734

735

736

737

738

739

740

741

742

743

744

Some caveats to our work require further studies. First, our light attenuation parameterization builds upon the empirical formulation of Ditoro (2001), previously validated for the Pearl River Estuary (PRE) through biogeochemical consistency checks (Wang et al., 2018). While this approach successfully captured observed oxygen dynamics in our simulations, two key simplifications require explicit discussion. The current light attenuation parameterization in our model primarily accounts for the effects of chlorophyll and suspended sediments. Previous studies have demonstrated that CDOM (colored dissolved organic matter) also plays a significant role in light attenuation within the PRE (Cao et al., 2003; Wang et al., 2010), particularly during algal bloom periods. Although our model does not explicitly treat CDOM as an independent variable, its influence is indirectly accounted for within the existing parameterization. However, to accurately quantify CDOM's contribution to oxygen dynamics—including its long-term trends—future work should incorporate an explicit representation of CDOM's effects on light attenuation in the model, alongside sustained observational monitoring of CDOM. For example, aApart from anthropogenic activities, alterations in regional physical conditions aligning with climate changes such as wind and freshwater discharge could also regulate the long-term deoxygenation in coastal regions (Yu et al., 2015; Chen et al., 2024). Besides, tThe impacts of ocean warming on deoxygenation (Laurent et al., 2018) remain unclear in the PRE as well, although warming has already been observed in the PRE (Cheung et al., 2021). Its compounding factors such as sea-level rise (Hong et al., 2020) may introduce additional complexity to hypoxia evolution through cascading ecosystem effects.

While these factors have not been considered in this study, the relative contributions of human activities and climate changes represent a significant topic for future investigations, which can facilitate a more comprehensive understanding of oxygen dynamics and hypoxia development in estuaries and coastal systems.

5. Conclusion

745

746

747

748

749

750

751

752

753

754

755

756

757

758

759

760

761

762

763

764

765

766

767

768

769

770

771

We applied a well-validated physical-biogeochemical model to reconstruct the summertime oxygen distributions in the PRE during two representative periods (the 1990s and the 2010s) and to disentangle the contribution of alterations in riverine inputs (i.e., suspended sediments, nutrients, and oxygen concentration) to the long-term deoxygenation off the PRE based on a suite of model experiments. We found that owing to the changes of riverine inputs over the past three decades, the low-oxygen and hypoxic areas in the bottom waters of the PRE have expanded by about 1.5 times and two-fold, respectively, with the duration time prolonged by ~15-35 days in summer. Concurrently, three hypoxic centers dominated by distinct factors were identified. Scenario simulations revealed that the decline in riverine oxygen concentration has caused a low-oxygen expansion (by ~44%) in the upper PRE. By comparison, the alterations in riverine nutrients and suspended sediments have separately provided better nutrient and light conditions to promote higher production of labile organic matter, which jointly maintained considerable oxygen depletions and exacerbated the low-oxygen conditions in the lower PRE. The relative importance of the changing riverine nutrients and suspended sediments to deoxygenation varied between subregions. The suspended sediment reduction was the predominated factor in the downstream regions close to the river outlets (e.g. the Modaomen sub-estuary), while the nutrient increase exerted a more substantial influence in the regions far from the river outlets (e.g. the Hong Kong waters). Our study highlights the significant role of the declined suspended sediments in the low-oxygen expansion off the PRE, which can further amplify the effect in association with the increasing nutrients. Therefore, in the

context of global regimes changes of riverine suspended sediments, we call for an urgent re-evaluation of the impacts of riverine inputs on deoxygenation in addition to nutrients in order to better understand the mechanism controlling hypoxia and thereby proposing effective mitigation strategies.

776

777

782

786

790

772

773

774

775

CRediT authorship contribution statement

- Yue Nan: Investigation, Model experiments, Formal analysis, Visualization,
- 779 Writing-original draft. **Zheng Chen:** Model experiments, Writing-review. **Bin Wang:**
- 780 Writing-review. Bo Liang: Writing-review. Jiatang Hu: Project administration,
- 781 Supervision, Conceptualization, Writing-review & editing.

Declaration of competing interest

- The authors declare that they have no known competing financial interests or
- personal relationships that could have appeared to influence the work reported in this
- 785 paper.

Acknowledgements

- This work was supported by a grant from the Southern Marine Science and
- 788 Engineering Guangdong Laboratory (Zhuhai) (Project. SML2023SP220) and two
- 789 consulting projects (ZB-2023-005, ZB-2023-054) to JH.

Data availability

791 The dissolved oxygen observation datasets off the Pearl River Estuary were 792 obtained from published studies (Hu et al., 2021, DOI: 10.5194/bg-18-5247-2021; Su 2017, DOI: 10.5194/bg-14-4085-2017; Li et al., 793 2021, DOI: 10.1029/2020JC016700) and the Hong Kong Environmental Protection Department 794 795 (www.epd.gov.hk). The observed nutrients, oxygen, and suspended sediments data in 796 the Pearl River are available from Hu et al. (2021) and publicly accessible databases 797 maintained by China's Ministry of Ecology and Environment (https://www.mee.gov.cn/) and the China River Sediment Bulletin (http://www.mwr.gov.cn/sj/tjgb/zghlnsgb/). 798

9 Data will be made available on request.

802 Reference

- 803 Barbosa, A. B., Domingues, R. B., and Galvão, H. M.: Environmental Forcing of
- 804 Phytoplankton in a Mediterranean Estuary (Guadiana Estuary, South-western Iberia):
- A Decadal Study of Anthropogenic and Climatic Influences, Estuaries and Coasts, 33,
- 806 324-341, 10.1007/s12237-009-9200-x, 2010.
- Bianchi, T. S., DiMarco, S. F., Cowan, J. H., Hetland, R. D., Chapman, P., Day, J. W.,
- and Allison, M. A.: The science of hypoxia in the Northern Gulf of Mexico: A review,
- 809 Science of The Total Environment, 408, 1471-1484,
- 810 https://doi.org/10.1016/j.scitotenv.2009.11.047, 2010.
- Breitburg, D., Levin, L. A., Oschlies, A., Grégoire, M., Chavez, F. P., Conley, D. J.,
- 812 Garçon, V., Gilbert, D., Gutiérrez, D., Isensee, K., Jacinto, G. S., Limburg, K. E.,
- Montes, I., Naqvi, S. W. A., Pitcher, G. C., Rabalais, N. N., Roman, M. R., Rose, K. A.,
- 814 Seibel, B. A., Telszewski, M., Yasuhara, M., and Zhang, J.: Declining oxygen in the
- global ocean and coastal waters, Science, 359, eaam7240, 10.1126/science.aam7240,
- 816 2018.
- 817 Bussi, G., Darby, S. E., Whitehead, P. G., Jin, L., Dadson, S. J., Voepel, H. E.,
- Vasilopoulos, G., Hackney, C. R., Hutton, C., Berchoux, T., Parsons, D. R., and
- Nicholas, A.: Impact of dams and climate change on suspended sediment flux to the
- 820 Mekong delta, Science of The Total Environment, 755, 142468,
- 821 https://doi.org/10.1016/j.scitotenv.2020.142468, 2021.
- 822 Cao, W., Yang, Y., Xu, X., Huang, L., and Zhang, J.: Regional patterns of particulate
- spectral absorption in the Pearl River estuary, Chinese Science Bulletin, 48, 2344-2351,
- 824 2003.
- 825 Cao, Z., Duan, H., Ma, R., Shen, M., and Yang, H.: Remarkable effects of greening
- 826 watershed on reducing suspended sediment flux in China's major rivers, Science
- 827 Bulletin, 68, 2285-2288, 2023.
- 828 Carstensen, J., Andersen, J. H., Gustafsson, B. G., and Conley, D. J.: Deoxygenation of
- the Baltic Sea during the last century, Proceedings of the National Academy of Sciences
- of the United States of America, 111, 5628-5633, 10.1073/pnas.1323156111, 2014.
- 831 Chen, J. Y., Pan, D. L., Liu, M. L., Mao, Z. H., Zhu, Q. K., Chen, N. H., Zhang, X. Y.,
- 832 and Tao, B. Y.: Relationships Between Long-Term Trend of Satellite-Derived
- 833 Chlorophyll-a and Hypoxia Off the Changjiang Estuary, ESTUARIES AND COASTS,
- 834 40, 1055-1065, 10.1007/s12237-016-0203-0, 2017.
- 835 Chen, L., Zhang, X., He, B., Liu, J., Lu, Y., Liu, H., Dai, M., Gan, J., and Kao, S.-J.:
- 836 Dark Ammonium Transformations in the Pearl River Estuary During Summer, Journal
- 837 of Geophysical Research: Biogeosciences, 125, e2019JG005596,
- 838 https://doi.org/10.1029/2019JG005596, 2020.
- 839 Chen, Z., Yu, L., and Hu, J.: Disentangling the contributions of anthropogenic nutrient
- input and physical forcing to long-term deoxygenation off the Pearl River Estuary,
- 841 China, Water Research, 265, 122258, https://doi.org/10.1016/j.watres.2024.122258,
- 842 2024.

- Cheung, Y. Y., Cheung, S., Mak, J., Liu, K., Xia, X., Zhang, X., Yung, Y., and Liu, H.:
- 844 Distinct interaction effects of warming and anthropogenic input on diatoms and
- dinoflagellates in an urbanized estuarine ecosystem, Global Change Biology, 27, 3463-
- 846 3473, 10.1111/gcb.15667, 2021.
- Cormier, J. M., Coffin, M. R. S., Pater, C. C., Knysh, K. M., Gilmour, R. F., Guyondet,
- 848 T., Courtenay, S. C., and van den Heuvel, M. R.: Internal nutrients dominate load and
- drive hypoxia in a eutrophic estuary, Environmental Monitoring and Assessment, 195,
- 850 1211, 10.1007/s10661-023-11621-y, 2023.
- 851 Cullen, J. J.: Subsurface Chlorophyll Maximum Layers: Enduring Enigma or Mystery
- 852 Solved?, in: ANNUAL REVIEW OF MARINE SCIENCE, VOL 7, edited by: Carlson,
- 853 C. A., and Giovannoni, S. J., 207-239, 10.1146/annurev-marine-010213-135111, 2015.
- 854 Dethier, E. N., Renshaw, C. E., and Magilligan, F. J.: Rapid changes to global river
- 855 suspended sediment flux by humans, Science, 376, 1447-1452,
- 856 10.1126/science.abn7980, 2022.
- 857 Diaz, R. J. and Rosenberg, R.: Spreading dead zones and consequences for marine
- 858 ecosystems, Science, 321, 926-929, 10.1126/science.1156401, 2008.
- 859 DiToro, D. M.: Sediment flux modeling, John Wiley & Sons2001.
- 860 Domingues, R. B., Barbosa, A. B., Sommer, U., and Galvão, H. M.: Phytoplankton
- 861 composition, growth and production in the Guadiana estuary (SW Iberia): Unraveling
- changes induced after dam construction, Science of The Total Environment, 416, 300-
- 863 313, https://doi.org/10.1016/j.scitotenv.2011.11.043, 2012.
- Fizpartick, J.: A user's guide for RCA (release 3.0), HydroQual Inc., New Jersey, USA.
- 865 217p, 2004.
- 866 Ge, J., Torres, R., Chen, C., Liu, J., Xu, Y., Bellerby, R., Shen, F., Bruggeman, J., and
- 867 Ding, P.: Influence of suspended sediment front on nutrients and phytoplankton
- 868 dynamics off the Changjiang Estuary: A FVCOM-ERSEM coupled model experiment,
- 869 Journal of Marine Systems, 204, 103292,
- 870 https://doi.org/10.1016/j.jmarsys.2019.103292, 2020.
- Hagy, J. D., Boynton, W. R., and Jasinski, D. A.: Modelling phytoplankton deposition
- 872 to Chesapeake Bay sediments during winter-spring: interannual variability in relation
- 873 to river flow, ESTUARINE COASTAL AND SHELF SCIENCE, 62, 25-40,
- 874 10.1016/j.ecss.2004.08.004, 2005.
- Hong, B., Liu, Z., Shen, J., Wu, H., Gong, W., Xu, H., and Wang, D.: Potential physical
- 876 impacts of sea-level rise on the Pearl River Estuary, China, Journal of Marine Systems,
- 877 201, 103245, 10.1016/j.jmarsys.2019.103245, 2020.
- Howarth, R., Chan, F., Conley, D. J., Garnier, J., Doney, S. C., Marino, R., and Billen,
- 6: Coupled biogeochemical cycles: eutrophication and hypoxia in temperate estuaries
- and coastal marine ecosystems, Frontiers in Ecology and the Environment, 9, 18-26,
- 881 https://doi.org/10.1890/100008, 2011.
- Hu, J. and Li, S.: Modeling the mass fluxes and transformations of nutrients in the Pearl
- 883 River Delta, China, Journal of Marine Systems, 78, 146-167,
- 884 https://doi.org/10.1016/j.jmarsys.2009.05.001, 2009.

- Hu, J., Li, S., and Geng, B.: Modeling the mass flux budgets of water and suspended
- sediments for the river network and estuary in the Pearl River Delta, China, Journal of
- 887 Marine Systems, 88, 252-266, https://doi.org/10.1016/j.jmarsys.2011.05.002, 2011.
- 888 Hu, J., Zhang, Z., Wang, B., and Huang, J.: Long-term spatiotemporal variations in and
- 889 expansion of low-oxygen conditions in the Pearl River estuary: a study synthesizing
- 890 observations during 1976–2017, Biogeosciences, 18, 5247-5264, 10.5194/bg-18-5247-
- 891 2021, 2021.
- 892 Huang, Y.-G., Yang, H.-F., Jia, J.-J., Li, P., Zhang, W.-X., Wang, Y. P., Ding, Y.-F., Dai,
- 893 Z.-J., Shi, B.-W., and Yang, S.-L.: Declines in suspended sediment concentration and
- 894 their geomorphological and biological impacts in the Yangtze River Estuary and
- 895 adjacent sea, Estuarine, Coastal and Shelf Science, 265, 107708,
- 896 https://doi.org/10.1016/j.ecss.2021.107708, 2022.
- 897 Kasai, M., Brierley, G. J., Page, M. J., Marutani, T., and Trustrum, N. A.: Impacts of
- land use change on patterns of sediment flux in Weraamaia catchment, New Zealand,
- 899 CATENA, 64, 27-60, https://doi.org/10.1016/j.catena.2005.06.014, 2005.
- Lai, Y., Jia, Z., Xie, Z., Li, S., and Hu, J.: Water quality changes and shift in mechanisms
- 901 controlling hypoxia in response to pollutant load reductions: A case study for Shiziyang
- 902 Bay, Southern China, Science of The Total Environment, 842, 156774
- 903 https://doi.org/10.1016/j.scitotenv.2022.156774, 2022.
- 904 Laurent, A., Fennel, K., Ko, D. S., and Lehrter, J.: Climate change projected to
- exacerbate impacts of coastal eutrophication in the northern Gulf of Mexico, Journal of
- 906 Geophysical Research: Oceans, 123, 3408-3426, 2018.
- 907 Li, D., Gan, J., Hui, R., Liu, Z., Yu, L., Lu, Z., and Dai, M.: Vortex and Biogeochemical
- 908 Dynamics for the Hypoxia Formation Within the Coastal Transition Zone off the Pearl
- River Estuary, Journal of Geophysical Research: Oceans, 125, 10.1029/2020jc016178,
- 910 2020a.
- 911 Li, D., Gan, J., Hui, C., Yu, L., Liu, Z., Lu, Z., Kao, S.-j., and Dai, M.: Spatiotemporal
- 912 Development and Dissipation of Hypoxia Induced by Variable Wind-Driven Shelf
- 913 Circulation off the Pearl River Estuary: Observational and Modeling Studies, Journal
- 914 of Geophysical Research: Oceans, 126, e2020JC016700,
- 915 https://doi.org/10.1029/2020JC016700, 2021.
- 916 Li, G., Liu, J., Diao, Z., Jiang, X., Li, J., Ke, Z., Shen, P., Ren, L., Huang, L., and Tan,
- 917 Y.: Subsurface low dissolved oxygen occurred at fresh- and saline-water intersection of
- 918 the Pearl River estuary during the summer period, Marine Pollution Bulletin, 126, 585-
- 919 591, 10.1016/j.marpolbul.2017.09.061, 2018.
- 920 Li, X., Lu, C., Zhang, Y., Zhao, H., Wang, J., Liu, H., and Yin, K.: Low dissolved
- 921 oxygen in the Pearl River estuary in summer: Long-term spatio-temporal patterns,
- 922 trends, and regulating factors, Marine Pollution Bulletin, 151, 110814,
- 923 https://doi.org/10.1016/j.marpolbul.2019.110814, 2020b.
- 924 Liu, Z., Fagherazzi, S., Liu, X., Shao, D., Miao, C., Cai, Y., Hou, C., Liu, Y., Li, X., and
- 925 Cui, B.: Long-term variations in water discharge and sediment load of the Pearl River
- 926 Estuary: Implications for sustainable development of the Greater Bay Area, Frontiers

- 927 in Marine Science, 9, 983517, 10.3389/fmars.2022.983517, 2022.
- 928 Lu, Z., Gan, J., Dai, M., Liu, H., and Zhao, X.: Joint Effects of Extrinsic Biophysical
- 929 Fluxes and Intrinsic Hydrodynamics on the Formation of Hypoxia West off the Pearl
- 930 River Estuary, Journal of Geophysical Research: Oceans, 123, 6241-6259,
- 931 10.1029/2018jc014199, 2018.
- 932 Luo, X., Yang, Q., and Jia, L.: The Riverbed Evolution of the River-Network System
- 933 in the Pearl River Delta, Sun Yat-sen Univeristy Press, Guangzhou, China, 2002.
- Ma, C., Zhao, J., Ai, B., Sun, S., and Yang, Z.: Machine Learning Based Long-Term
- 935 Water Quality in the Turbid Pearl River Estuary, China, Journal of Geophysical
- 936 Research: Oceans, 127, e2021JC018017, https://doi.org/10.1029/2021JC018017, 2022.
- 937 Ma, R., Chen, Z., Wang, B., Xu, C., Jia, Z., Li, L., and Hu, J.: Spatiotemporal variations
- and controlling mechanism of low dissolved oxygen in a highly urbanized complex
- 939 river system, Journal of Hydrology: Regional Studies, 52, 101691,
- 940 https://doi.org/10.1016/j.ejrh.2024.101691, 2024.
- 941 Murphy, R. R., Kemp, W. M., and Ball, W. P.: Long-Term Trends in Chesapeake Bay
- 942 Seasonal Hypoxia, Stratification, and Nutrient Loading, ESTUARIES AND COASTS,
- 943 34, 1293-1309, 10.1007/s12237-011-9413-7, 2011.
- 944 Pitcher, G. C., Aguirre-Velarde, A., Breitburg, D., Cardich, J., Carstensen, J., Conley,
- 945 D. J., Dewitte, B., Engel, A., Espinoza-Morriberón, D., Flores, G., Garçon, V., Graco,
- 946 M., Grégoire, M., Gutiérrez, D., Hernandez-Ayon, J. M., Huang, H.-H. M., Isensee, K.,
- 947 Jacinto, M. E., Levin, L., Lorenzo, A., Machu, E., Merma, L., Montes, I., Swa, N.,
- 948 Paulmier, A., Roman, M., Rose, K., Hood, R., Rabalais, N. N., Salvanes, A. G. V.,
- 949 Salvatteci, R., Sánchez, S., Sifeddine, A., Tall, A. W., Plas, A. K. v. d., Yasuhara, M.,
- 250 Zhang, J., and Zhu, Z. Y.: System controls of coastal and open ocean oxygen depletion,
- 951 Progress in Oceanography, 197, 102613, https://doi.org/10.1016/j.pocean.2021.102613,
- 952 2021.
- 953 Roman, M. R., Brandt, S. B., Houde, E. D., and Pierson, J. J.: Interactive effects of
- 954 Hypoxia and temperature on coastal pelagic zooplankton and fish, Frontiers in Marine
- 955 Science, 6, 10.3389/fmars.2019.00139, 2019.
- 956 Su, J., Dai, M., He, B., Wang, L., Gan, J., Guo, X., Zhao, H., and Yu, F.: Tracing the
- origin of the oxygen-consuming organic matter in the hypoxic zone in a large eutrophic
- estuary: the lower reach of the Pearl River Estuary, China, Biogeosciences, 14, 4085-
- 959 4099, 10.5194/bg-14-4085-2017, 2017.
- 960 Syvitski, J. P. M. and Kettner, A.: Sediment flux and the Anthropocene, Philosophical
- Transactions of the Royal Society A: Mathematical, Physical and Engineering Sciences,
- 962 369, 957-975, doi:10.1098/rsta.2010.0329, 2011.
- Wang, B., Hu, J., Li, S., and Liu, D.: A numerical analysis of biogeochemical controls
- 964 with physical modulation on hypoxia during summer in the Pearl River estuary,
- 965 Biogeosciences, 14, 2979-2999, 10.5194/bg-14-2979-2017, 2017.
- Wang, B., Hu, J., Li, S., Yu, L., and Huang, J.: Impacts of anthropogenic inputs on
- 967 hypoxia and oxygen dynamics in the Pearl River estuary, Biogeosciences, 15, 6105-
- 968 6125, 10.5194/bg-15-6105-2018, 2018.

- Wang, G., Cao, W., Yang, Y., Zhou, W., Liu, S., and Yang, D.: Variations in light
- 970 absorption properties during a phytoplankton bloom in the Pearl River estuary,
- 971 Continental Shelf Research, 30, 1085-1094, 2010.
- 972 Wang, H., Dai, M., Liu, J., Kao, S.-J., Zhang, C., Cai, W.-J., Wang, G., Qian, W., Zhao,
- 973 M., and Sun, Z.: Eutrophication-Driven Hypoxia in the East China Sea off the
- 974 Changjiang Estuary, Environmental Science & Technology, 50, 2255-2263,
- 975 10.1021/acs.est.5b06211, 2016.
- Wang, J. J., Bouwman, A. F., Liu, X. C., Beusen, A. H. W., Van Dingenen, R., Dentener,
- 977 F., Yao, Y. L., Glibert, P. M., Ran, X. B., Yao, Q. Z., Xu, B. C., Yu, R. C., Middelburg,
- 978 J. J., and Yu, Z. G.: Harmful Algal Blooms in Chinese Coastal Waters Will Persist Due
- 979 to Perturbed Nutrient Ratios, ENVIRONMENTAL SCIENCE & TECHNOLOGY
- 980 LETTERS, 8, 276-284, 10.1021/acs.estlett.1c00012, 2021.
- 981 Wang, K., Chen, J., Jin, H., Li, H., Gao, S., Xu, J., Lu, Y., Huang, D., Hao, Q., and
- 982 Weng, H.: Summer nutrient dynamics and biological carbon uptake rate in the
- 983 Changjiang River plume inferred using a three end-member mixing model, Continental
- 984 Shelf Research, 91, 192-200, https://doi.org/10.1016/j.csr.2014.09.013, 2014.
- Wang, Y., Wu, H., Lin, J., Zhu, J., Zhang, W., and Li, C.: Phytoplankton Blooms off a
- 986 High Turbidity Estuary: A Case Study in the Changjiang River Estuary, Journal of
- 987 Geophysical Research: Oceans, 124, 8036-8059, 10.1029/2019jc015343, 2019.
- 988 Wen, G., Liang, Z., Xu, X., Cao, R., Wan, Q., Ji, G., Lin, W., Wang, J., Yang, J., and
- 989 Huang, T.: Inactivation of fungal spores in water using ozone: Kinetics, influencing
- 990 factors and mechanisms, Water Research, 185, 116218,
- 991 https://doi.org/10.1016/j.watres.2020.116218, 2020.
- Wu, C. S., Yang, S., Huang, S., and Mu, J.: Delta changes in the Pearl River estuary and
- its response to human activities (1954–2008), Quaternary International, 392, 147-154,
- 994 https://doi.org/10.1016/j.quaint.2015.04.009, 2016.
- 995 Yang, H., Wang, T., Yang, D., Yan, Z., Wu, J., and Lei, H.: Runoff and sediment effect
- of the soil-water conservation measures in a typical river basin of the Loess Plateau,
- 997 CATENA, 243, 108218, https://doi.org/10.1016/j.catena.2024.108218, 2024.
- 998 Yu, L., Gan, J., 2022. Reversing impact of phytoplankton phosphorus limitation on
- 999 coastal hypoxia due to interacting changes in surface production and shoreward bottom
- oxygen influx. Water Res. 118094 https://doi.org/10.1016/j. watres.2022.118094.
- 1001 Yu, L., Fennel, K., Laurent, A., 2015. A modeling study of physical controls on hypoxia
- generation in the northern Gulf of Mexico. J. Geophys. Res. Oceans 120, 5019–5039.
- 1003 https://doi.org/10.1002/2014JC010634.
- 1004 Yu, L., Gan, J., Dai, M., Hui, C., Lu, Z., Li, D., 2020. Modeling the role of riverine
- organic matter in hypoxia formation within the coastal transition zone off the Pearl
- 1006 River Estuary. Limnol. Oceanogr. 9999, 1–17. https://doi.org/10.1002/lno.11616
- Zhang, S., Lu, X. X., Higgitt, D. L., Chen, C.-T. A., Han, J., and Sun, H.: Recent
- 1008 changes of water discharge and sediment load in the Zhujiang (Pearl River) Basin,
- 1009 China, Global and Planetary Change, 60, 365-380,
- 1010 https://doi.org/10.1016/j.gloplacha.2007.04.003, 2008.

Zhang, Z., Wang, B., Li, S., Huang, J., and Hu, J.: On the Intra-annual Variation of Dissolved Oxygen Dynamics and Hypoxia Development in the Pearl River Estuary, Estuaries and Coasts, 45, 1305-1323, 10.1007/s12237-021-01022-0, 2022.